

---

# The Local Interaction Basis: Identifying Computationally-Relevant and Sparsely Interacting Features in Neural Networks

---

Lucius Bushnaq\* Stefan Heimersheim Nicholas Goldowsky-Dill Dan Braun† Jake Mendel

Kaarel Hänni‡ Avery Griffin§ Jörn Stöhler§ Magdalena Wache§

Marius Hobbahn¶

Apollo Research

## Abstract

Mechanistic interpretability aims to understand the behavior of neural networks by reverse-engineering their internal computations. However, current methods struggle to find clear interpretations of neural network activations because a decomposition of activations into computational features is missing. Individual neurons or model components do not cleanly correspond to distinct features or functions. We present a novel interpretability method that aims to overcome this limitation by transforming the activations of the network into a new basis - the Local Interaction Basis (LIB). LIB aims to identify computational features by removing irrelevant activations and interactions. Our method drops irrelevant activation directions and aligns the basis with the singular vectors of the Jacobian matrix between adjacent layers. It also scales features based on their importance for downstream computation, producing an interaction graph that shows all computationally-relevant features and interactions in a model. We evaluate the effectiveness of LIB on modular addition and CIFAR-10 models, finding that it identifies more computationally-relevant features that interact more sparsely, compared to principal component analysis. However, LIB does not yield substantial improvements in interpretability or interaction sparsity when applied to language models. We conclude that LIB is a promising theory-driven approach for analyzing neural networks, but in its current form is not applicable to large language models.

## 1 Introduction

Mechanistic Interpretability aims to understand the internals of neural networks and to reverse engineer computation inside neural networks [Olah et al., 2017, Elhage et al., 2021]. Previous attempts have analyzed toy models [Chughtai et al., 2023, Nanda et al., 2023a] or circuits that compute specific subtasks performed by large language models [Olah et al., 2020, Meng et al., 2023, Geiger et al., 2021, Wang et al., 2022, Conmy et al., 2024]. These analyses largely rely on interpretations of model components [Wang et al., 2022], individual neurons [Gurnee et al., 2023], or

---

\*Correspondence to Lucius Bushnaq <lcus@apolloresearch.ai>

†Lead Engineer

‡Cadenza Labs

§Independent

¶See Section 5 for contributions

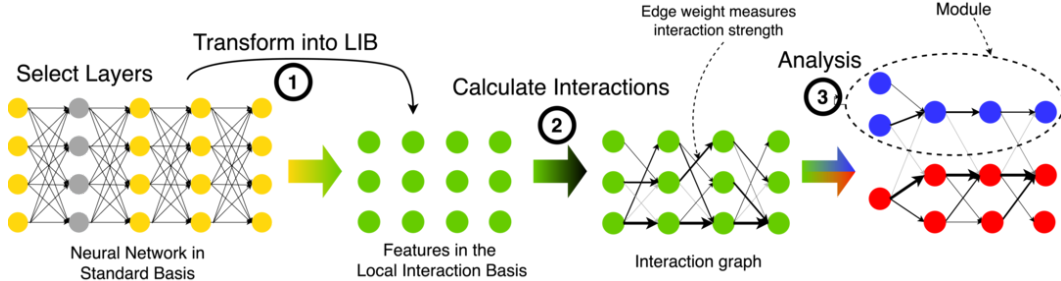


Figure 1: The Local Interaction Basis (LIB) is a basis for neural network activations where interactions between features should be sparser and more modular. (1) We start with a selection of layers from the neural network. (2) We transform the activations in these layers into the LIB, which represents computationally-relevant features, removes features that don’t affect the output, and minimizes interactions between features in adjacent layers. (3) We then quantify the interactions between features using integrated gradients, creating an interaction graph that represents the extent to which preceding nodes affect subsequent nodes. (4) We use the resulting interaction graph to analyze and interpret features in the neural network, and to identify modules that correspond to distinct circuits in the model’s computation.

principal components [Millidge and Black, 2022]. Other approaches to disentangling the features learned in the latent spaces of the network include Schmidhuber [1992], Desjardins et al. [2012], Kim and Mnih [2018], Chen et al. [2016], Peebles et al. [2020], Schneider and Vlachos [2021]; see Bengio et al. [2014] for a review.

However, it has become clear that the standard basis (aligned with activation basis directions, sometimes referred to as “neuron basis”) is not the right unit for interpretability due to polysemanticity: neurons [Olah et al., 2017, Nguyen et al., 2016, Goh et al., 2021, Geva et al., 2021] and model components [e.g. attention heads, Janiak et al., 2023] do not correspond to individual features. Yet there is evidence that features are linearly represented in the activation space of neural networks [Nanda et al., 2023a, Gurnee et al., 2023, Nanda et al., 2023b]. Therefore, there are two possibilities for how features are represented in neural networks: (a) the model has more features than dimensions, but these features are sparsely activating represented in superposition [Elhage et al., 2022, Sharkey et al., 2022, Vaintrob et al., 2024], or (b) features are represented in a non-overcomplete basis, but not aligned with neurons.<sup>1</sup> While option (a) has some merits [interpretability results, see Cunningham et al., 2023, Bricken et al., 2023, Marks et al., 2024], its drawback is a higher complexity. We therefore focus on testing option (b) and present a method that assumes a non-overcomplete basis of features.

Our work introduces two novel contributions to the field of mechanistic interpretability. First, we develop the Local Interaction Basis (LIB), a method for finding a more interpretable basis for neural network activations. LIB builds upon the theoretical framework proposed by Bushnaq et al. [2024a], which aims to find a parameterization-invariant representation of neural networks. The key idea is that the standard basis representation of a neural network’s parameters contains superfluous structure that hinders interpretability. Our method removes degenerate directions in layer activations and in gradients between adjacent layers. This yields simpler but equivalent representation of the network, containing only computationally-relevant features—features that are relevant for downstream computation. The LI basis is aligned with singular vectors of the Jacobian between layers such that LIB features are sparsely interacting, and ordered by their effect on the next layer.

Second, we propose the use of integrated-gradient interaction graphs to analyze the relationships between features in the LIB-transformed network. Integrated gradients [IGs, Friedman, 2004] have been previously used to attribute neural network outputs to inputs [Sundararajan et al., 2017], and recently been applied to sparse autoencoder features [Marks et al., 2024]. We employ IGs to represent the full network as an interaction graph to reveal hidden structure in neural networks. IGs are particularly well-suited for this purpose due to their desirable properties, including implementation

<sup>1</sup>Intermediate options are also a possibility: For example, the model’s activation space could be split into different subspaces, some of which contain more sparsely activating features than the dimension of the subspace, while others contain non-sparse features and do not have more features than dimensions.

invariance, completeness, sensitivity, linearity [Sundararajan et al., 2017], and robustness to basis transformations [Bushnaq et al., 2024b].

We apply our method to two toy models and two language models. We transform activations into the LI basis and summarize the network as an interaction graph. We successfully isolate computationally-relevant features in the modular addition and CIFAR-10 toy models and are able to interpret model features based on the interaction graphs. We find that the method does not work well on language models (Tinystories-1M and GPT2-small): while the LI basis is more sparsely-interacting than the PCA baseline in some cases, the interactions remain relatively dense and the features are no more interpretable.

In this paper, we describe the LIB method, our IG-based interaction graph, and our graph analysis methods (Section 2). We apply the new tools to a modular addition transformer, an MLP trained on CIFAR 10, and two language models (GPT2-small and Tinystories-1M) and present the results in Section 3. We conclude in Section 4.

## 2 Methodology

Our interpretability method represents a network in a new basis which better captures its computational structure. We expect that these new basis directions correspond to meaningful features of the model, enabling us to interpret individual features and feature interactions across the network. Our method involves three key steps: first, transforming activations into a local interaction basis (LIB, Section 2.1); second, computing integrated-gradient attributions (Section 2.2); and third, creating and analyzing an interaction graph to identify modules (Section 2.3). Figure 1 provides an overview of this process, below we provide details on each step.

**Select layers to analyze:** The first step is to choose a subset of layers of the neural network to include in the LIB interaction graph. To see the connection structure of the network, graph layers should usually be chosen close to each other, e.g. after every attention and MLP layer in a transformer. We index layers of the LIB graph with  $l = 1, \dots, l_{\text{final}}$ .

1. **Transform into local interaction basis:** We apply a linear transformation to bring the activations into the LI basis (illustrated in Figure 2):
  - (a) Transformation into the PCA (principal component analysis) basis: In each layer, we calculate the principal components of the activation vectors collected over the dataset and transform into a basis aligned with these principal components.
  - (b) Transformation to the LI basis: We iterate through the chosen network layers, in order from the closest to the outputs to the closest to the inputs. In every layer, we compute how much every direction in a layer “connects” to every direction in the following layer by calculating a Jacobian matrix: the gradients of LIB features in the following layer with respect to directions in the current layer. Then we transform into a basis aligned with the right-handed singular vectors of the Jacobian.
2. **Calculate interaction edges:** We build an *interaction graph*, a graph of all LIB features in the network with edges representing the strength of interaction between features in adjacent layers. The interaction strength between two features is computed by calculating integrated gradients-based attributions [Sundararajan et al., 2017] on every data point and then taking the quadratic mean over the dataset.
3. **Analyze the graph:** We test the sparsity of interactions (by ablating interactions), cluster the graph into modules, and interpret the nodes.

### 2.1 Step 1: The Local Interaction Basis (LIB)

In this section, we describe the LIB transformation. LIB is based on a predecessor, the (global) interaction basis described in Bushnaq et al. [2024a] and Appendix E; here we describe the local interaction basis and provide a concrete implementation. The two types of architectures we consider here are MLPs and transformers (see Appendices A.1 through A.3 for model details). In both cases we reformulate the architectures such that they can be written as a sequential composition of layers (concatenating the residual stream and component activations of transformers), and such that every

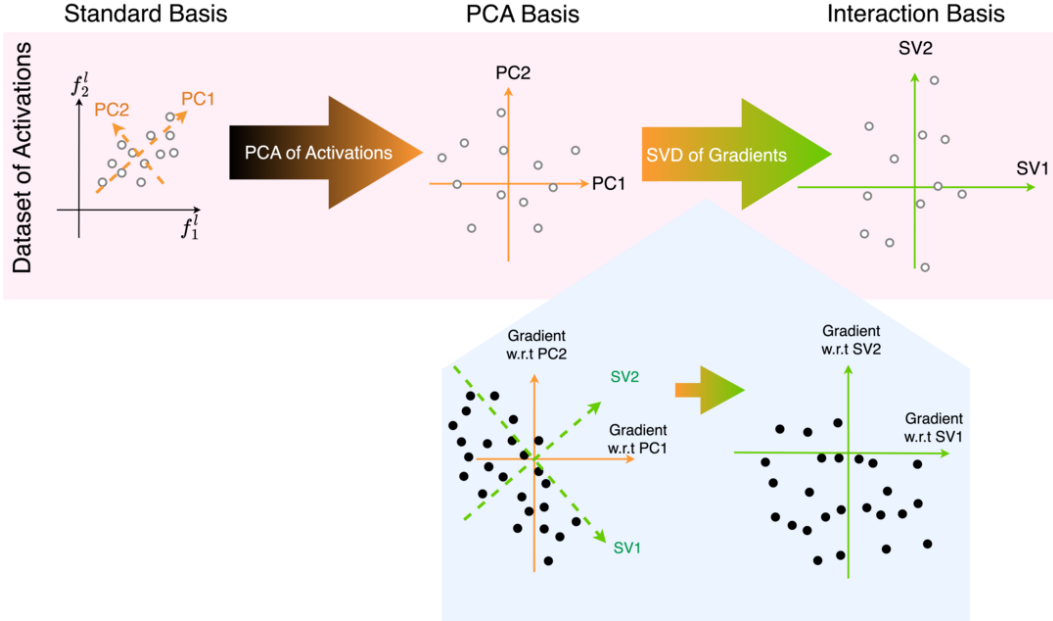


Figure 2: Visualization of the LIB transformation. This figure shows an illustration of activations (top) and gradients (bottom) as they get transformed into the LIB. The first step is a PCA of the activations in every layer in order to drop activation directions with near-zero variance and to whiten the activations. The second step is based on a dataset of gradients, that is, the set of gradients of every feature in the next layer with respect to every direction in the current layer on every data point (this is a larger dataset than the activations). We perform an SVD (singular value decomposition) on the Jacobians to find the right singular vectors and singular values. This allows us to drop directions that are not important for the next layer, and to align the activations singular vectors to sparsify the interactions between features in adjacent layers.

layer returns zero if its input is zero (we fold-in the biases). We describe these adjustments in Sections A.4 and A.5, respectively.

The codebase implementing LIB and our integrated gradient computation is available at <https://github.com/ApolloResearch/rib>, and we provide the pseudocode for the basic algorithms in Appendix D.

The transformation  $\hat{\mathbf{f}}^l = C^l \mathbf{f}^l$  to change into the LIB is best understood as consisting of two sequential linear transformations: a transformation into the PCA basis of the activations, followed by a transformation into the basis of right singular vectors of the Jacobian matrix to the next layer.

The first transformation into the PCA basis consists of four steps. We (i) center the activations over the dataset and calculate principal components and values, and (ii) rotate the activations into a basis aligned with its principal components. Then we (iii) drop directions with near-zero principal values, and (iv) rescale the remaining directions with a diagonal matrix such that their covariance matrix is the identity. We give a precise mathematical description in appendix B.1.

The purpose of this first transformation is mainly to drop irrelevant directions (those with near-zero variance), and to whiten the activations as a preparation for the second transformation.

For the second transformation we compute the Jacobians  $J_{ij}^l(x)$ , the gradient of the  $i$ -th feature in layer  $l + 1$  with respect to the  $j$ -th feature in layer  $l$  for every data point  $x$ . We then compute the singular value decomposition (SVD) of the  $n_{\text{data}} d^{l+1} \times d^l$  dimensional all-data Jacobian matrix (a flattening of the 3-dimensional Jacobian tensor along the  $x$  and  $i$  indices) and save the right singular vectors and singular values. One might think of this as taking a PCA of the set of all the Jacobian rows (for all  $i$  and  $x$ ) except without centering. We (i) rotate the activations into a basis aligned with these right singular vectors, (ii) drop directions with near-zero eigenvalues, and (iii) rescale the activations with corresponding singular values. We give a precise mathematical description in Appendix B.2.

The second rotation achieves multiple goals. Firstly, we can drop directions in activation space that explain variance in the current layer (not dropped by first rotation) but have no influence on future layers (zero singular values). Secondly, the rotation into the SVD basis should make the interactions between features in adjacent layers as sparse as possible.<sup>2</sup> Finally, the multiplication by the singular values scales the features proportional to how important they are for the following layers.

This is a recursive process, starting from the final layer and working backwards. In that final layer we start the recursion by only applying the PCA step. Specifically we only perform mean-centering and alignment with PCA directions but not the rescaling. In addition to the recursion-based *local* interaction basis we also considered a global interaction basis where we apply the second transformation just with respect to the final layer, rather than the next layer. We describe this alternative approach, closer to the version proposed in Bushnaq et al. [2024a], in appendix E. We found that the results were similar, and decided to focus on LIB due to its lower computational cost.

Our transformer implementation needs to account for the token indices, in addition to the feature indices. This increases the computational cost of computing the Jacobians (which now depend on four rather than two indices). For this reason we introduce a approximation technique based on stochastic sources [Dong and Liu, 1994] which we find to provide accurate results in practice. We provide the equations for the transformer implementation in Appendix B.4, and describe the stochastic sources technique in Appendix C.

## 2.2 Step 2: Quantifying interactions with integrated gradients

In the previous subsection we derived a basis for the activations to identify the features in every layer. In this subsection we quantify the interaction strength between features in different layers.

We use integrated gradients [Friedman, 2004, Sundararajan et al., 2017] to attribute the influence of one feature onto another. The reason we choose this method is that it uniquely satisfies a set of properties we want from an attribution method: implementation invariance, completeness, sensitivity, linearity, and consistency under coordinate transformations [Bushnaq et al., 2024b].

Integrated gradients yield an attribution  $A_{i,j}^{l+1,l}(x)$  quantifying the influence of feature  $f_j^l$  in layer  $l$  on feature  $f_i^{l+1}$  in layer  $l + 1$ , at a given data point  $x$ :

$$A_{i,j}^{l+1,l}(x) := f_j^l(x) \int_0^1 d\alpha \left[ \frac{\partial}{\partial z_j^l} (F_i^{l+1,l}(\mathbf{z}^l)) \right]_{\mathbf{z}^l = \alpha \mathbf{f}^l(x)} \quad (1)$$

where  $F$  is the function that maps  $\mathbf{f}^l$  to  $\mathbf{f}^{l+1}$ ,  $F(\mathbf{f}^l(x)) = \mathbf{f}^{l+1}(x)$ .

To obtain averaged attributions  $E_{i,j}^{l+1,l}$  for the entire dataset, we take the RMS of the attributions for individual data points. We choose the RMS as the simplest way to average over the dataset<sup>3</sup> but other ways to average attributions may be considered in future work.

To speed up the computation of the attributions, we use the fact that the integral in equation (1) is linear in  $\mathbf{z}^l$  for elementwise activation functions (such as ReLU). Thus we can skip the integration in such cases, and just evaluate the integrand at  $\alpha = 1$ . For approximately linear activation functions (such as GELU) we find that this is still a good approximation and thus use this approximation throughout.

For transformer models, the activations vary with token index and data point, and activations of later tokens can depend on previous tokens. We generalize equation (1) by considering the influence of  $f_{j,t}^l(x)$  on  $f_{i,s}^{l+1}(x)$  (with token indices  $t$  and  $s$ ). Instead of taking the RMS over the dataset, we take the RMS summing over both, dataset index  $x$  and token index  $s$ . The dataset- and token-averaged

<sup>2</sup>The SVD basis for a *single* datapoint always gives the sparsest interactions. In our case we choose the SVD of the reshaped matrix, inspired by the procedure for higher-order SVD, as a guess of the best basis for the full dataset. We have not proven that this basis leads to sparsest interactions in all cases.

<sup>3</sup>The simplest way beyond simply summing attributions; a simple sum would lead to undesired cancellations between positive and negative attributions.

edge attribution formula for transformers is thus

$$E_{i,j}^{l+1,l} := \left( \frac{1}{|\mathcal{D}|} \frac{1}{T} \sum_{x \in \mathcal{D}} \sum_{s=1}^T \left( \sum_{t=1}^T f_{j,t}^l(x) \int_0^1 d\alpha \left[ \frac{\partial}{\partial z_{j,t}^l} \left( F_{i,s}^{l+1,l}(\mathbf{z}^l) \right) \right]_{\mathbf{z}^l = \alpha \mathbf{f}^l(x)} \right)^2 \right)^{1/2}. \quad (2)$$

As discussed in Section 2.1, calculating Jacobians for all indices  $i, j, s, t$  is computationally expensive and we apply stochastic sources to reduce the computational cost (see Appendix C).

### 2.3 Step 3: Interaction graph analysis

Based on the features and attributions between features, we create a layered graph. The nodes in the graph are the features in the network  $\hat{f}_j^l$  for  $j = 1, \dots, d^l$  in layer  $l$ , and the edges between a pair of features in adjacent layers are given by the averaged attributions  $\hat{E}_{i,j}^{l+1,l}$ .<sup>4</sup> We show examples of these graphs in Section 3.

We test the *sparsity* of the interactions by running edge ablations, implemented as follows: To measure the effect of ablating the edge  $\hat{E}_{i_0,j_0}^{l+1,l}$ , we compute a forward pass  $l \rightarrow l+1$  setting node  $\hat{f}_{j_0}^l$  to 0, and saving only the result for  $\hat{f}_{i_0}^{l+1}$ . Then, we compute another forward pass  $l \rightarrow l+1$  without ablating  $\hat{f}_{j_0}^l$ , saving the results for  $\hat{f}_i^{l+1}$ ,  $i \neq i_0$ . Finally, we combine these results to obtain the activations for layer  $l+1$  with the edge ablated, and pass them through the rest of the network. We can also ablate multiple edges at once by ablating a different subset of input nodes when computing the value of each output node. In that case we perform one forward pass for each node in layer  $l+1$  that requires a different input mask (up to  $d^{l+1}$  forward passes). As with most activation patching experiments [Vig et al., 2020, Geiger et al., 2021, Meng et al., 2023, Goldowsky-Dill et al., 2023], there is a risk that this method takes the network out of distribution in a somewhat unprincipled manner [Chan et al., 2022], but the technique is commonly used and seems to work in practice.

To test the sparsity of a layer in a given basis we sort all edges by their size  $\hat{E}_{i,j}^{l+1,l}$  and then remove as many edges as possible, starting with the smallest ones, while maintaining a given accuracy or loss. We implement this as a bisect search, and typically require on the order of 10-20 iterations to find the number of edges required to maintain the given accuracy/loss. This method relies on the edge size being a good proxy for the importance of an interaction, otherwise an important edge may be ablated while less important edges are kept.

Finally, we aim to find modules in the interaction graph as a way to identify circuits in the computation of the network. We are interested in modularity in the sense of graph sections that have comparatively low *node-connectivity* with the rest of the network. That is, the minimum number of nodes that need to be removed from the graph to disconnect two modules. However, we cannot cheaply compute the node-connectivity of the graph, so we use a modularity score which measures how many edges connect nodes in the same module compared to how many edges connect nodes in different modules. This is an approximation, and we see our modularity analysis as a first proof of concept rather than the definitive method. For more details see Bushnaq et al. [2024a].

In practice, we used the Leiden algorithm [Traag et al., 2019] for its speed and scalability. To emulate the effect of the node-connectivity, we set the edges passed to the Leiden algorithm to

$$\mathcal{E}_{i,j}^{l+1,l} = \log \left( \hat{E}_{i,j}^{l+1,l} / \epsilon \right) \quad (3)$$

where  $\epsilon$  is the smallest edge required to maintain a high level of accuracy (obtained via edge ablation experiments). The reasoning for the logarithmic scaling follows Bushnaq et al. [2024a]. The Leiden algorithm optimizes the community assignments  $c_i^l$  to maximize the modularity score

$$Q = \frac{1}{2m} \sum_{a,i,j} \left( \mathcal{E}_{i,j}^{l+1,l} - \frac{k_i^{l+1} k_j^l}{2m} \right) \delta(c_i^{l+1}, c_j^l). \quad (4)$$

where  $k_i^{l+1} = \sum_j \mathcal{E}_{i,j}^{l+1,l}$  and  $m = \sum_{i,j} \mathcal{E}_{i,j}^{l+1,l}$ .

<sup>4</sup>We are using  $\hat{E}$  to denote the attribution between LIB features  $\hat{\mathbf{f}}$ , rather than standard basis features.

### 3 Results

In this section, we show experimental results for a transformer trained on a modular addition task, a CIFAR-10 MLP, and two language models. We compare the LI basis to the PCA basis as a baseline.<sup>5</sup> We find the following:

1. LIB features are about as interpretable as PCA features (Sections 3.1 and 3.3), and more computationally-relevant (in the cases discussed in Sections 3.1 and 3.2).
2. Integrated gradient interaction graphs and modularity analyses can be useful for circuit discovery (Section 3.1 and 3.2).
3. LIB features are more sparsely interacting than PCA features in CIFAR-10 (Section 3.2) and most layers of the language models we tested (Section 3.3).

#### 3.1 Modular Addition Transformer

Modular addition is a well-studied task on which transformer models develop simple, human-interpretable algorithms [Nanda et al., 2023a, Chughtai et al., 2023, Zhong et al., 2023]. The task is to predict the result of the mathematical operation  $z = x + y \pmod p$  (for a fixed  $p = 113$  in our case). We train a transformer model on this task, see Appendix A.1 for details. Transformers tend to implement the “clock” algorithm [Nanda et al., 2023a] which calculates  $\cos(\omega(x + y + \phi))$  for various values of  $\omega$  and  $\phi$  and combines those to calculate  $z$ . A simple version of this algorithm would be to make the logit for output token  $a$  proportional to  $\cos(2\pi(x + y - a)/p)$ , for all outputs. Then the highest logit would always be the one where  $a = z = x + y \pmod p$ . In practice, models tend to use multiple frequencies  $< p$  to improve the confidence of the prediction.

This algorithm is particularly easy to visualize because we can use a Fourier transform to represent any neural network activation as a sum of sinusoidal terms of different frequencies (see Appendix F for details). In short, we decompose any feature into terms such as 70%  $\cos(7x + 7y) + 30\% \cos(31x + 31y)$  which means that 70% (and 30%) of the variance in that feature’s value can be explained by an oscillating function with frequency 7 (and 31) in the  $x + y$  direction. We use this notation to label LIB features and PCA features in the interaction graphs below.

We test whether LIB and PCA identify meaningful computational features of the algorithm, and how they compare. We do this by checking

- **Functional relevance:** All features found should be computationally-relevant to the output of the network. We check this based on their interactions with future layers.
- **Monosemanticity:** Features should mostly represent single Fourier frequencies.<sup>6</sup>
- **Sparsity:** Features should interact sparsely, i.e. there should be few edges of relevant size in our interaction graph. We operationalize this by checking how many edges we can ablate while retaining  $> 99.9\%$  test accuracy.
- **Modularity:** Is there modular structure in the interaction graph? For instance, is there a set of features that track a single set of frequencies and which interact much more strongly with each other than with other sets of features?<sup>7</sup>

We visualize results as an interaction graph as introduced in Section 2.3. Nodes in the graph are LIB features, split by layer, sorted by importance, and colored by module. In the modular addition interaction graphs, we set the edge line widths to be proportional to the squared interactions  $\hat{E}_{ij}^2$  to match the explained variance description. We also normalize the edges sizes per-layer to improve readability for the graph in the PCA basis.

<sup>5</sup>PCA suggests itself as a minimal baseline since LIB aims to be an improved version of PCA. However, SAEs are the interpretability method that currently yields the most human-interpretable results. Subjectively, we found that features found by SAEs are more human-interpretable than those found by LIB.

<sup>6</sup>We would expect good features before the attention layer to be largely mono-frequency because taking the product of two frequencies results in cross-terms that are not helpful for the modular addition algorithm. In later layers, in particular in the unembedding layer, features don’t necessarily have to be mono-frequency anymore.

<sup>7</sup>Note that we expect up to two pure features for every frequency. This is because there can be two independent terms that differ in their phase  $\phi$  but we omit this phase in the labeling.

We show the LIB interaction graph of a modular addition model in Figure 3. The plot only shows the directions and interactions needed to maintain 99.9% accuracy on the task. We can ablate most nodes (and even more interactions) while maintaining near-perfect model performance.

This model is cherry-picked (out of 5 models trained with different seeds) as our simplest modular addition model; LIB works particularly well on this model and the interaction graph is easy to understand. However we show quantitative results for all seeds in the following figures, and provide all interaction graphs (including PCA versions) in Appendix G.

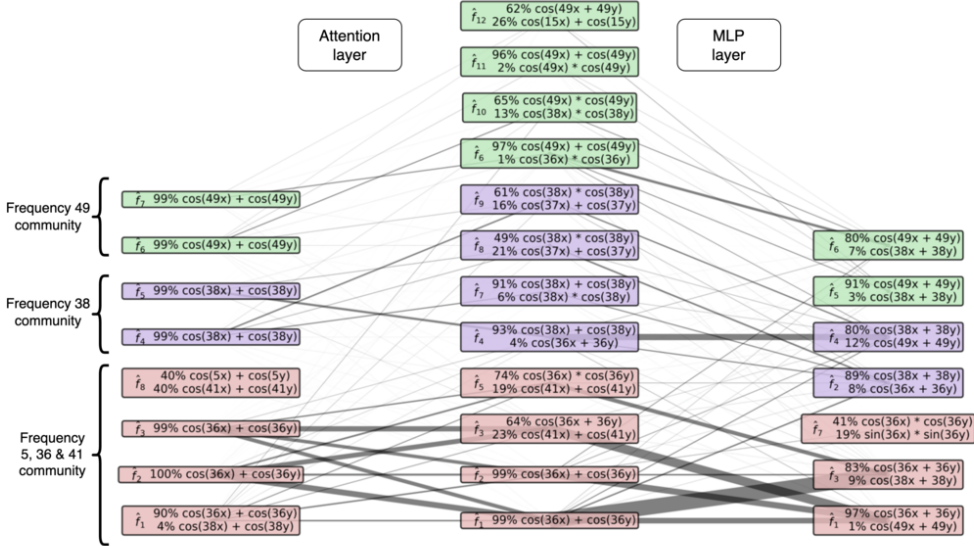


Figure 3: LIB interaction graph of a modular addition transformer. The three layers correspond to activations after the embedding, directly after the attention, and just before the unembedding. The individual nodes represent LIB features, and the thickness of the edges shows the interaction strength between features. The nodes are colored by module membership (Leiden algorithm), and labeled by their function index ( $\hat{f}_0, \hat{f}_1, \dots$ , in order of decreasing functional importance) and their Fourier interpretation.

### 3.1.1 Functional relevance

One advantage that LIB has over PCA is that it accounts for which features affect future layers and thus can ignore computationally-irrelevant features. For instance, if a direction explains a lot of variance in a layer’s activations but doesn’t affect future activations, then the PCA basis will include it but LIB will not.

We test this manually by checking whether the LIB or PCA basis contain features that appear irrelevant based in the interaction graph. We provide all interaction graphs and additional details in Appendix G. We find that in the final layer the PCA has a lot of computationally-irrelevant features, while LIB does not. In the middle layer, the effect is less strong, but we identify around 14 irrelevant features in the PCA basis and just 3 in the LIB basis (across the 5 seeds).

We conclude that when there are directions in the model’s activation spaces that are not computationally-relevant for the output but that explain a non-trivial fraction of the variance in a layer, LIB is better than PCA at excluding these directions.

### 3.1.2 Monosemanticity

As a proxy for feature interpretability, we test how monosemantic LIB and PCA features are. We measure monosemanticity as the fraction of variance in the activation of a feature is explained by a single Fourier term.

We find that LIB does not have a consistent advantage over PCA. Figure 4a shows the amount of variance explained by the first Fourier term in the first 10 basis directions. We find no difference in layers 1 and 2, but an advantage for LIB in layer 0. However, further investigation (Figure 4b) shows

that this is an outlier driven by seed-4 only. Thus we conclude that LIB features are not clearly more monosemantic than PCA features.

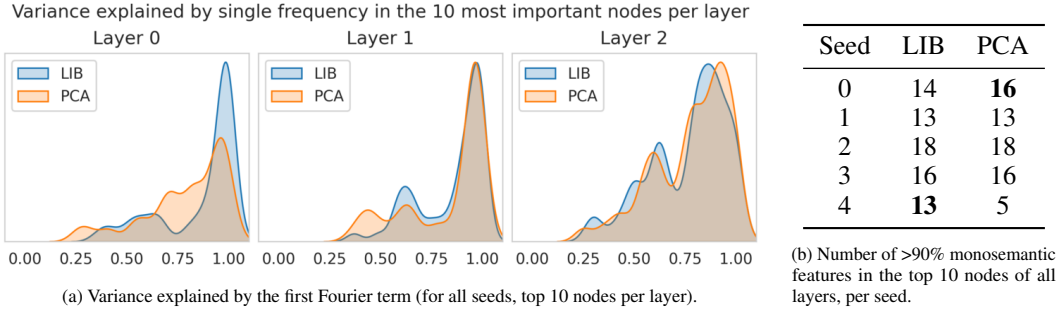


Figure 4: Monosemanticity of features in LIB and PCA basis.

### 3.1.3 Sparsity

The previous two sections analyzed the features of the LIB and PCA bases. Now we want to focus on the *interactions* between those features, as represented by the edges in the interaction graphs. We start by comparing the sparsity of interactions in the two bases in this section, and explore modularity in the next section.

To give some context on the interaction sparsity we briefly show the feature sparsity, i.e. the number of features we can ablate without losing much accuracy. Figure 5 shows ablation curves, accuracy as a function of remaining features (i.e. the left edge corresponds to all features being ablated). We show LIB (blue) and PCA (orange) for 5 models trained with different seeds. LIB tends to require slightly fewer features than PCA to maintain high accuracy, but the effect is very seed-dependent.

As our main metric for interaction sparsity we use edge ablations, as introduced in Section 2.3. Instead of ablating features, we ablate edges and measure the accuracy as a function of the number of edges ablated. Rather than showing the full edge ablation curves, we use the number of edges required to maintain 99.9% accuracy as a benchmark in the modular addition task. Other thresholds yield similar results.

We find mixed results, as shown in Figure 6. In the attention layer, the LI basis always requires fewer edges than the PCA basis, but in the MLP layer LIB is sparser in only 3 out of 5 models, while PCA is sparser in 2 models. We see the attention layer results as tentative evidence that LIB can find more sparsely interacting features than PCA, but the MLP results are not clear-cut and depend on the model seed.

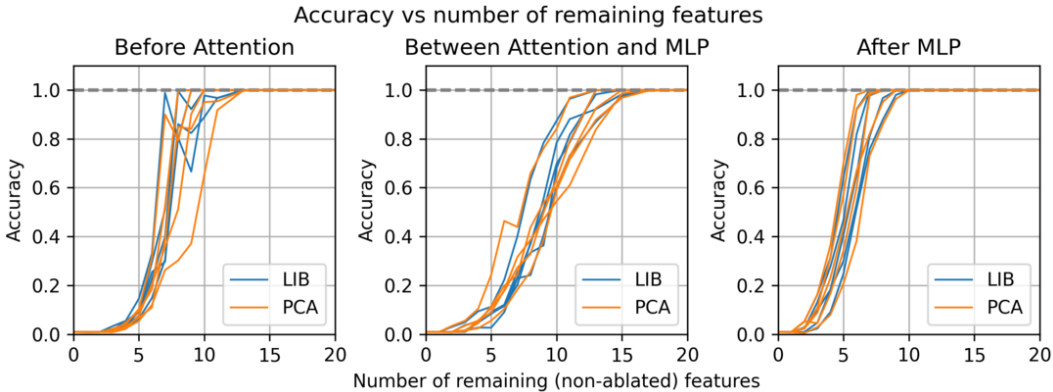


Figure 5: Number of nodes required to preserve >99.9% accuracy for LIB and PCA on five modular addition transformers trained with different random seeds.

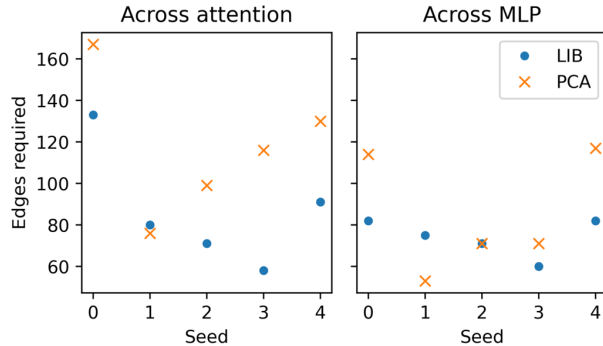


Figure 6: Number of edges required to preserve >99.9% accuracy for LIB and PCA on five modular addition transformers trained with different random seeds. Lower number of edges required is better, as it means the representation has sparser interactions. Across attention LIB is always sparser than PCA. Across the MLP the trend is unclear.

### 3.1.4 Modularity

Finally, we want to test whether our modularity algorithm as described in Section 2.3 can find meaningful modules in the interaction graph. Ideally we would want to see modules that cleanly separate the different frequencies used by the model (which we expect to not interact much with each other).

We find that this works sometimes but not reliably. Figure 3 shows a cherry-picked example (with fine-tuned resolution parameter  $\gamma = 0.5$ , rather than the default  $\gamma = 1$ ) where we find that the modules mostly separate out the different frequencies used by the model (the most important frequencies are 49, 38, and 36). Other models (Appendix G) show less clear-cut modules. Overall, we conclude that the modularity algorithm we use does not achieve our goals reliably.

## 3.2 CIFAR-10 MLP

As another simple test case, we apply LIB to small fully connected networks trained on CIFAR-10 [Krizhevsky, 2009, see Appendix A.2 for details]. We train 5 different models with different random seeds with consistent results; in this section we present results from seed-0 unless otherwise noted.

Our models achieve 46.6% - 48.4% test accuracy on CIFAR-10. This is on par with other 2-layer fully connected MLPs without data augmentation, but only somewhat better than pixel-based logistic regression (41% accuracy) [Lin et al., 2015]. Basic CNNs can achieve much higher accuracy (e.g. Krizhevsky et al. [2012] achieve 87% accuracy), but adapting LIB to CNNs is out of scope for this paper. Given its architecture, we expect our MLP model to use basic heuristics such as hue and brightness, rather than relationships between neighboring pixels (which e.g. curve detectors require).

In this section, we compare the LI basis and PCA basis in two ways: We compare how sparsely features in different layers interact with each other (as in Section 3.1.3), and we analyze how well both bases isolate a specific interpretable feature we found, the vehicle-vs-animal feature.

### 3.2.1 Sparsity

To judge the sparsity of interactions between the features in adjacent layers we again use the edge ablation test (see Section 2.3). We measure how many interactions between features can be ablated while maintaining a classification accuracy that is within 0.1 percentage points of the original model’s accuracy.

We find that, for all layers and seeds, interactions in the LI basis are sparser than in the PCA basis. Figure 8 shows the number of edges required, and we find that LIB always requires fewer edges than the PCA basis.

Note that despite the somewhat dense looking graph in Figure 7, we need very few edges (just 25 connecting each pair of layers) to preserve good performance.

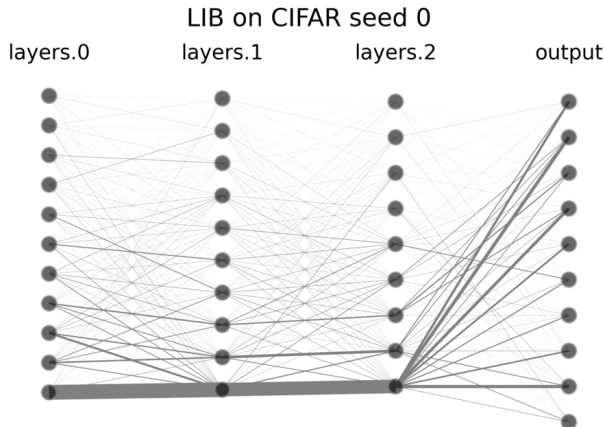


Figure 7: LIB interaction graph for our CIFAR model (seed-0). The four layers correspond to input, first hidden, second hidden, and output layer. Edges width corresponds to squared-edges, as this makes the graph more readable.

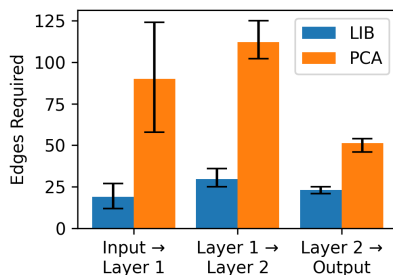


Figure 8: Edge ablation comparison between LIB and PCA on CIFAR-10. The plot shows the minimum number of edges required to maintain an accuracy within 0.1 percentage points of the original model. Lower values indicate sparser interactions. The colored bars represent the mean across 5 random seeds, with the error bars indicating the minimum and maximum values across seeds.

### 3.2.2 Animal vs Vehicle Direction

In Figure 7, the LIB interaction graph, we see a path of thick edges at the bottom, indicating features which interact strongly with each other compared to other features in the network, and affect the output substantially. On inspection we notice that these features are all involved in distinguishing animals from vehicles. This is a core subtask on CIFAR-10 (containing 5 animal classes and 5 vehicle classes), and our model is reasonably good at it; summing the output probabilities across these categories gives a classifier with an AUROC of 0.946 (88.2% accuracy).

LIB finds a single direction in the model at each layer that is almost solely responsible for this subtask, including in the ‘pixel space’ in the input layer. This is an example of LIB successfully finding directions that are computationally-relevant for downstream parts of the model. If we use the direction in the final layer as a linear probe, it is nearly as good of a classifier as the model itself, with an AUROC of 0.932.

In Figure 9 we show the AUROC of the top four LIB and PCA features as animal/vehicle classifiers, to judge how well the animal/vehicle distinction is concentrated to a single feature. We find that the animal-vs-feature direction is clearly isolated in the LI basis, but not in the PCA basis. In the PCA basis it is spread out over several directions.

We test whether our explanation of this direction as an animal-vs-vehicle feature is correct, we perform two tests. First, we measure what fraction of variance in this direction is explained by the animal-vs-vehicle label, and find that the label only explains 54% of the variance. This could be either because the feature has a second function, or because the remaining variance is due to noise. To test this we intervene on the feature, “correcting” the activation by setting it to the mean

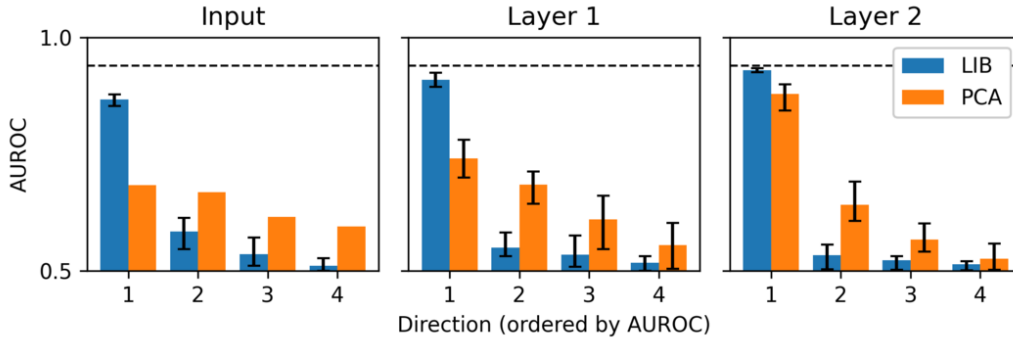


Figure 9: Comparison of how well LIB and PCA isolate the animal-vs-vehicle feature into a single basis direction. The four bars show the best animal-vs-vehicle classifying directions in each basis (measured by AUROC, again mean with errorbars indicating minimum and maximum values across 5 seeds). The dashed black line is the AUROC of the full model’s output. LIB isolates the feature into a single direction, while PCA spreads it out over several directions.

value of activations with the true animal/vehicle label. We find that this *improves* the model, with accuracy increasing from 47.6% to 54.6%. This is evidence that our interpretation of the feature as an animal-vs-vehicle feature is correct.

### 3.3 Language Models

Finally, we apply the LIB method to language models, GPT2-small [Radford et al., 2019] and TinyStories-1M [Eldan and Li, 2023]. We describe model and dataset details in Appendix A.3. We focus on GPT2-small here because it is the larger model. Our results for TinyStories-1M are similar or better than for GPT2-small, and shown in Appendix I.

In this section, we show interpretations for some of the LIB features (Section 3.3.1) and feature interactions (Section 3.3.2), and test the sparsity and modularity of the graphs (Section 3.3.3).

#### 3.3.1 Interpretability of LIB directions

We analyze a selection of LIB directions in GPT2-small to understand if they track meaningful and interpretable features.

We find that we can successfully interpret the first 4 LIB directions, which track positional features. We also show feature visualizations for a random selection of other LIB directions, but find them to be not particularly interpretable.

The results we find for the PCA basis are very similar to these LIB results and we omit them from this section. This means the second rotation does not seem to aid interpretability, as we hoped it might.

**Positional features:** We noticed that several directions in the LIB and PCA basis of GPT2-small seem to represent positional information. We show this in Figure 10 where we plot the activations of the first 4 LIB directions as a function of sequence position. We show the 6th block activations as an example, but the plot is similar for throughout most layers of the model. We find that around 97% of the variance in these four directions is explained by the sequence position. The first direction seems to represent a “is this position 0?” feature, the second direction just scales with the sequence index, and the third and fourth directions represent a sinusoidal function of the sequence index. The latter two directions explain the helix-like structure in GPT2-small that has been noted before [e.g. Yedidia, 2023].

**Language features:** To visualize directions in activation space we show dataset examples that activate the feature by a given amount. Our visualization is based on `sae_vis` [McDougall, 2024], but modified because our features, unlike features from standard sparse autoencoders, can be both positive and negative. We show the minimum and maximum activating dataset examples, as well as

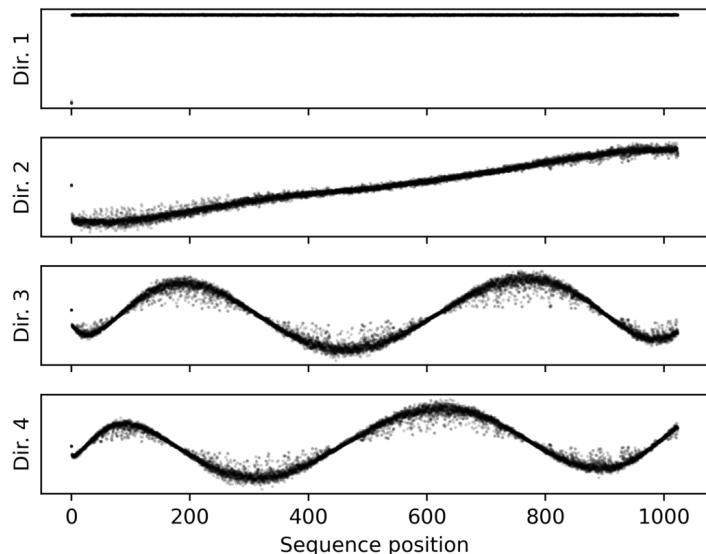


Figure 10: Positional features in GPT2-small. The activations of the first four LIB directions as a function of sequence index.

four intervals of intermediate-activating examples. We again show features in the 6th block of GPT2-small (specifically at the very beginning of the block) but the results for other blocks are qualitatively similar. We host feature visualizations for a random selection of LIB and PCA features of all layers at [https://data.apolloresearch.ai/lib/feature\\_viz/](https://data.apolloresearch.ai/lib/feature_viz/). Below we provide screenshots for a selection of LIB directions.

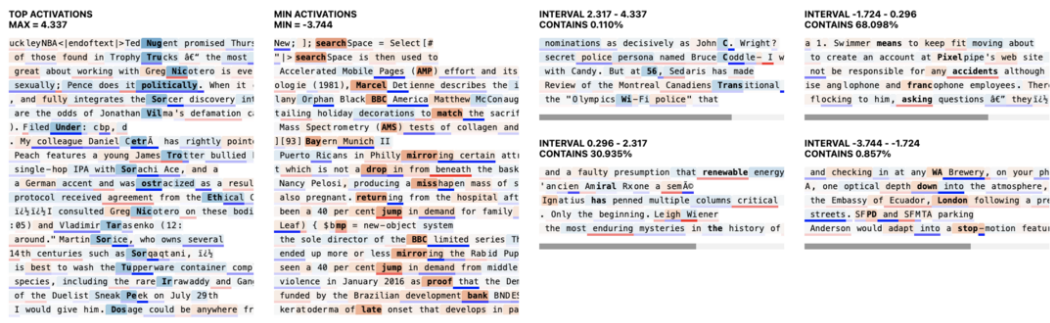


Figure 11: LIB feature 105 at the beginning of the 6th block of GPT2-small.

As an example of a somewhat interpretable direction we show feature 105 in Figure 11. The feature seems to maximally activate on the first token of last names and brand names (“Ted Nugent”, “Greg Nicotero”, “Tupperware”), and we also see two such examples in the first quartile samples (“John C. Wright”, “Bruce Coddle”). However, we also see other samples that do not follow this rule.

One worry we have is that the maximum and minimum activating examples are dominated by outliers in the dataset, and not indicative of the meaning of the direction. As an example of this we show feature 109 in Figure 12. Most of the top activating examples are the word “Hawk” in the name of a particular graphics card, and other top activations are last names starting with H. Minimally activating examples are mostly the token “cos” and similar tokens. However, none of these interpretations explain the dataset examples that cause intermediate activations, showing that the interpretation based on top-activating samples is not predictive and likely not correct. Possible ways to improve this include computing feature activations on custom prompts designed to test an interpretation, and using more intermediate samples. A detailed interpretability analysis however is out of scope for this paper. In Appendix H we show more visualizations of three more randomly selected LIB features.

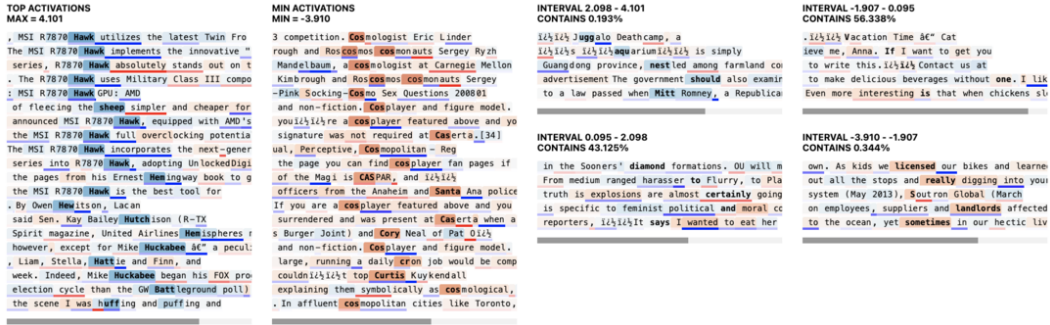


Figure 12: LIB feature 109 at the beginning of the 6th block of GPT2-small.

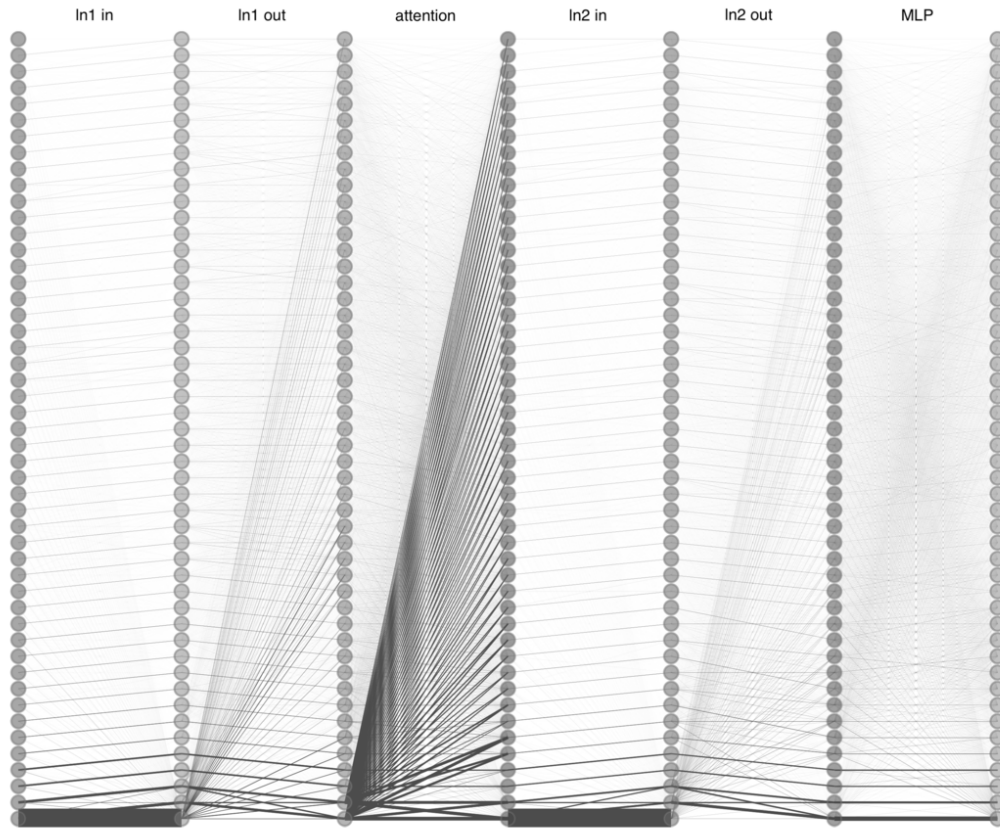


Figure 13: The LIB interaction graph at a representative block in the middle of GPT2-small (block 6). All edges have been square-root normalized. Only the first 50 nodes in each layer are shown. The size of the two largest edges have been clipped to make the graph readable.

Overall we find that the LIB features are not particularly interpretable. This is comparable to what we find for PCA directions (not shown here but available at this [url](#)).

### 3.3.2 Interpretability of interactions

We use the interaction graph to analyze the interactions between LIB features in GPT2-small. We show one transformer block of the graph in Figure 13. We have arbitrarily chosen transformer block 6, but the other blocks look similar. Out of the six sets of edges shown, two correspond to attention and MLP layers, while the remaining four are related to layer norm (two layer norms, each split into two sets of edges). We provide a diagram of our transformer architecture in Appendix A.4.

We find that the edges corresponding to layer norms are mostly 1-to-1 connections. The only exceptions are the connections to and from the variance feature. The variance feature is influenced by all input features, but most strongly by the first LIB feature (edges labeled “In1 in” and “In2 in” in Figure 13). As we saw in Section 3.3.1, this feature is a “is this the 0th position in the sequence”-feature. This explains its outsized effect on the variance feature because the 0th position is treated uniquely in GPT2 and has an unusually large norm. The variance feature is also connected to all output features (edges labeled “In1 out” and “In2 out” in Figure 13). This is expected because the variance in layer norm scales the output in every direction.

Looking at the edges across the attention module, we see the first two input features have a strong connection to most of the output features. These input features are a binary representation of “is this position 0?” and a linear representation of “sequence index” respectively (see Section 3.3.1). The LIB graph claims that these input features are influential on most output features of the attention block. This is expected because we know that the attention mechanism often depends on the token position.

Apart from these two observations about positional information, we cannot make much sense of the interaction graph. In particular the edges across Attention and MLP layers are relatively dense and did not permit straightforward interpretation with manual inspection.

### 3.3.3 Sparsity

We run our edge-ablation test again (see Section 2.3) to measure how many edges we can ablate while maintaining a cross-entropy loss within 0.1 of the original model. This is a relatively large loss increase; we do not claim that a 0.1 loss increase is inessential but merely use it as an (arbitrary) threshold to compare the sparsity of the LIB and PCA bases.

We show the results in Figure 14. We find that, in both bases, we can ablate 80 to 95% of the interactions while keeping the loss increase below 0.1. We can ablate slightly more interactions using LIB compared to PCA but the results are noisy. LIB tends to give sparser interactions than PCA in some early attention layers and in most MLP layers.

In Appendix I we run the same test for the much-smaller TinyStories-1M model and find that LIB is consistently sparser than PCA in the attention and MLP layers of TinyStories-1M, as shown in Figure 22b. For the TinyStories-1M model we were able to use a larger dataset to compute the LIB and PCA bases. These results suggest that either LIB works better on the smaller model, or that the larger dataset improved the quality of the LI basis. We do not test LIB on GPT2-small with a larger dataset because even if we achieved sparsity improvements similar to Figure 22b, say increasing the number of interactions we can ablate from  $\sim 80\%$  to  $\sim 90\%$ , we would still not consider this result good enough to achieve our goals. LIB would very likely not enable qualitatively different interpretability work or fine-grained modularity analysis on GPT2-small.

For completeness, we also show results for non-attention and non-MLP layers in appendix I. The results for those layers are mixed, with very different results between GPT2-small and TinyStories-1M. However, we think that results for those layers are less relevant, as they just represent the layer norm layers and are very sparse in both PCA and LIB basis.

## 4 Conclusion

We developed a novel interpretability method based on a transformation to the local interaction basis (LIB) and integrated gradient interaction graphs. Our work is built on the theoretical work by [Bushnaq et al. \[2024a\]](#) who propose representations based on parameterization-invariant structures in neural networks. LIB assumes that features in a neural network can be represented in a non-overcomplete basis. Additionally we assume that the main sources of freedom in the loss-landscape are linear dependencies in the activations of individual layers, and linear dependencies in the gradients between adjacent layers. LIB attempts to find a basis of sparsely interacting features for the activations of a neural network, represent the interactions between features in a graph, and identify modularity in the network’s computations by searching for modules in this graph.

We find that our method produces more interpretable and more sparsely-interacting representations on toy models (a modular addition transformer and a CIFAR-10 model), compared to a baseline of using PCA directions as features. On language models, we find that LIB produces more sparsely-interacting representations than PCA in some layers, but the representations are not more interpretable.

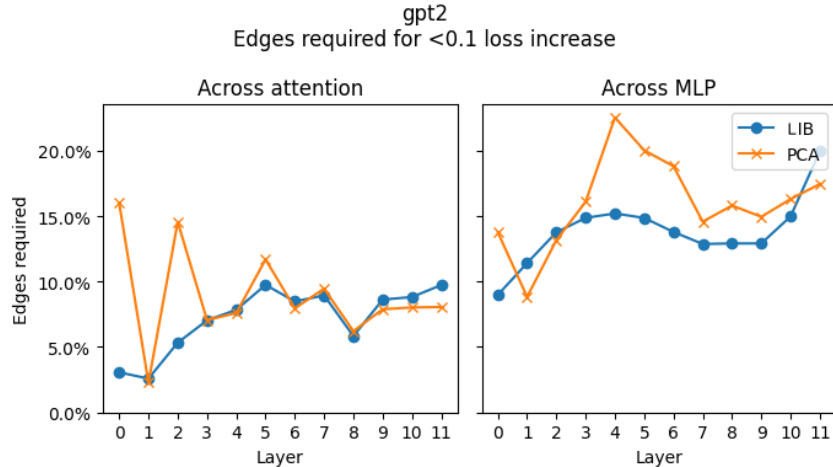


Figure 14: Edge ablation results on GPT2-small, for both LIB and PCA interaction graphs. We ablate as many edges as possible without increasing the cross-entropy loss by more than 0.1. The fewer edges, the better since this implies a sparser interaction graph.

Furthermore, we do not find evidence of modularity in the interaction graphs produced by LIB on language models.

Our goal was to test whether LIB could find a basis of features that would be more interpretable and interact much more sparsely than baseline methods (PCA). We conclude that, while promising on toy models, LIB does not achieve this goal on language models. We speculate that the assumption of a linear non-overcomplete basis was wrong in the case of LMs, and is the reason for not finding interpretable and sparsely-interacting features.

While our test of the LIB method yielded a negative result, we are still excited about future work building other methods based on the theory-framework [Bushnaq et al., 2024a]. In particular, we are interested in developing a generalization of LIB to the case of overcomplete bases to allow for the possibility of the network representing features in superposition using sparse coding.

## 5 Contribution Statement

**Theory** Lucius Bushnaq led the theory development, working on the conceptual framework, motivation and LIB methodology before anyone else joined the project. Jake Mendel provided extensive red-teaming and development of the methodology via theoretical arguments and experimental counterexamples. Kaarel Hänni first proposed the use of integrated gradients and contributed substantially to refinements of the theory.

**Infrastructure** Dan Braun led development of the current codebase, with significant contributions from Nix Goldowsky-Dill and Stefan Heimersheim. This replaced much earlier versions by Jörn Stöhler, Avery Griffin and Marius Hobbhahn. Nix Goldowsky-Dill and Dan Braun scaled the implementation to LLMs. Nix Goldowsky-Dill implemented the edge ablation experiments. Stefan Heimersheim implemented most of the supported bases and interaction metrics. The main experiments were run by Stefan Heimersheim and Nix Goldowsky-Dill.

**Analysis** Much of the analysis of earlier versions of LIB was performed by Marius Hobbhahn on a modular addition transformer, an MNIST MLP, and GPT2-small, with support from Avery Griffin and Jörn Stöhler. Of the analysis that this manuscript is based on, Stefan Heimersheim led the analysis of the Modular Addition Transformer and Nix Goldowsky-Dill led the analysis of the CIFAR10 model. Stefan Heimersheim and Nix Goldowsky-Dill contributed equally to the analysis of the language models.

**Paper Writing** The manuscript was primarily written by Stefan Heimersheim. Sections 1 and 2 were drafted by Lucius Bushnaq and Jake Mendel with extensive contributions by Marius Hobbhahn. The experiment section was drafted by Stefan Heimersheim (modular addition and LLM feature

visualization) and Nix Goldowsky-Dill (CIFAR and LLM positional features). Diagrams were created by Jake Mendel and Stefan Heimersheim.

**Leadership** Lucius Bushnaq coordinated the team, leading the high-level direction around which experiments to run. Stefan Heimersheim coordinated the writing of this manuscript. Marius Hobbhahn acted as a hands-on advisor, managing the team and giving regular feedback throughout the project and the writing of this manuscript.

## 6 Acknowledgements

We are grateful to James Fox, Jacob Hilton, Tom McGrath, and Lawrence Chan for feedback on this manuscript. Apollo Research is a fiscally sponsored project of Rethink Priorities.

## References

- Yoshua Bengio, Aaron Courville, and Pascal Vincent. Representation learning: A review and new perspectives, 2014.
- Trenton Bricken, Adly Templeton, Joshua Batson, Brian Chen, Adam Jermyn, Tom Conerly, Nick Turner, Cem Anil, Carson Denison, Amanda Askell, Robert Lasenby, Yifan Wu, Shauna Kravec, Nicholas Schiefer, Tim Maxwell, Nicholas Joseph, Zac Hatfield-Dodds, Alex Tamkin, Karina Nguyen, Brayden McLean, Josiah E Burke, Tristan Hume, Shan Carter, Tom Henighan, and Christopher Olah. Towards monosemanticity: Decomposing language models with dictionary learning. *Transformer Circuits Thread*, 2023. <https://transformer-circuits.pub/2023/monosemantic-features/index.html>.
- Lucius Bushnaq, Jake Mendel, Kaarel Hänni, Dan Braun, Nicholas Goldowsky-Dill, Stefan Heimersheim, Avery Griffin, Jörn Stöhler, Magdalena Wache, and Marius Hobbhahn. Degeneracy in the loss landscape can be used to identify the algorithm implemented by a neural network, May 2024a. URL [https://publications.apolloresearch.ai/degeneracy\\_loss\\_landscape\\_interpretability](https://publications.apolloresearch.ai/degeneracy_loss_landscape_interpretability).
- Lucius Bushnaq, Jake Mendel, Kaarel Hänni, and Stefan Heimersheim. Interpretability: Integrated gradients is a decent attribution method, May 2024b. URL [https://publications.apolloresearch.ai/integrated\\_gradients\\_criteria](https://publications.apolloresearch.ai/integrated_gradients_criteria).
- Lawrence Chan, Adria Garriga-Alonso, Nix Goldowsky-Dill, Ryan Greenblatt, Jenny Nishinskaya, Ansh Radhakrishnan, Buck Shlegeris, and Nate Thomas. Causal scrubbing: A method for rigorously testing interpretability hypotheses. Alignment Forum, 2022. URL <https://www.alignmentforum.org/posts/JvZhhzyHu2Yd57RN/causal-scrubbing-a-method-for-rigorously-testing>.
- Xi Chen, Yan Duan, Rein Houthoofd, John Schulman, Ilya Sutskever, and Pieter Abbeel. InfoGAN: Interpretable representation learning by information maximizing generative adversarial nets. *Advances in neural information processing systems*, 29, 2016.
- Bilal Chughtai, Lawrence Chan, and Neel Nanda. A Toy Model of Universality: Reverse Engineering How Networks Learn Group Operations. *arXiv e-prints*, art. arXiv:2302.03025, February 2023. doi: 10.48550/arXiv.2302.03025.
- Bilal Chughtai, Lawrence Chan, and Neel Nanda. A toy model of universality: Reverse engineering how networks learn group operations. In *International Conference on Machine Learning*, pages 6243–6267. PMLR, 2023.
- Arthur Conmy, Augustine Mavor-Parker, Aengus Lynch, Stefan Heimersheim, and Adrià Garriga-Alonso. Towards automated circuit discovery for mechanistic interpretability. *Advances in Neural Information Processing Systems*, 36, 2024.
- Hoagy Cunningham, Aidan Ewart, Logan Riggs, Robert Huben, and Lee Sharkey. Sparse autoencoders find highly interpretable features in language models. *arXiv preprint arXiv:2309.08600*, 2023.

- Guillaume Desjardins, Aaron Courville, and Yoshua Bengio. Disentangling factors of variation via generative entangling. *arXiv preprint arXiv:1210.5474*, 2012.
- Shao-Jing Dong and Keh-Fei Liu. Stochastic estimation with z2 noise. *Physics Letters B*, 328 (1–2):130–136, May 1994. ISSN 0370-2693. doi: 10.1016/0370-2693(94)90440-5. URL [http://dx.doi.org/10.1016/0370-2693\(94\)90440-5](http://dx.doi.org/10.1016/0370-2693(94)90440-5).
- Ronen Eldan and Yuanzhi Li. Tinstories: How small can language models be and still speak coherent english? *arXiv preprint arXiv:2305.07759*, 2023.
- Nelson Elhage, Neel Nanda, Catherine Olsson, Tom Henighan, Nicholas Joseph, Ben Mann, Amanda Askell, Yuntao Bai, Anna Chen, Tom Conerly, Nova DasSarma, Dawn Drain, Deep Ganguli, Zac Hatfield-Dodds, Danny Hernandez, Andy Jones, Jackson Kernion, Liane Lovitt, Kamal Ndousse, Dario Amodei, Tom Brown, Jack Clark, Jared Kaplan, Sam McCandlish, and Chris Olah. A mathematical framework for transformer circuits. *Transformer Circuits Thread*, 2021. <https://transformer-circuits.pub/2021/framework/index.html>.
- Nelson Elhage, Tristan Hume, Catherine Olsson, Nicholas Schiefer, Tom Henighan, Shauna Kravec, Zac Hatfield-Dodds, Robert Lasenby, Dawn Drain, Carol Chen, Roger Grosse, Sam McCandlish, Jared Kaplan, Dario Amodei, Martin Wattenberg, and Christopher Olah. Toy models of superposition. *Transformer Circuits Thread*, 2022. [https://transformer-circuits.pub/2022/toy\\_model/index.html](https://transformer-circuits.pub/2022/toy_model/index.html).
- Eric Friedman. Paths and consistency in additive cost sharing. *International Journal of Games Theory*, 32:501–518, 08 2004. doi: 10.1007/s001820400173.
- Atticus Geiger, Hanson Lu, Thomas Icard, and Christopher Potts. Causal abstractions of neural networks. *Advances in Neural Information Processing Systems*, 34:9574–9586, 2021.
- Mor Geva, Roei Schuster, Jonathan Berant, and Omer Levy. Transformer Feed-Forward Layers Are Key-Value Memories, September 2021. URL <http://arxiv.org/abs/2012.14913>. arXiv:2012.14913 [cs].
- Gabriel Goh, Nick Cammarata †, Chelsea Voss †, Shan Carter, Michael Petrov, Ludwig Schubert, Alec Radford, and Chris Olah. Multimodal neurons in artificial neural networks. *Distill*, 2021. doi: 10.23915/distill.00030.
- Aaron Gokaslan and Vanya Cohen. Openwebtext corpus. <http://Skylion007.github.io/OpenWebTextCorpus>, 2019.
- Nicholas Goldowsky-Dill, Chris MacLeod, Lucas Sato, and Aryaman Arora. Localizing Model Behavior with Path Patching. *arXiv e-prints*, art. arXiv:2304.05969, April 2023. doi: 10.48550/arXiv.2304.05969.
- Wes Gurnee, Neel Nanda, Matthew Pauly, Katherine Harvey, Dmitrii Troitskii, and Dimitris Bertsimas. Finding neurons in a haystack: Case studies with sparse probing, 2023.
- Jett Janiak, Chris Mathwin, and Stefan Heimersheim. Polysemantic attention head in a 4-layer transformer, Nov 2023. URL <https://www.alignmentforum.org/posts/nuJFTS5iiJKT5G5yh/polysemantic-attention-head-in-a-4-layer-transformer>.
- Hyunjik Kim and Andriy Mnih. Disentangling by factorising. In *International conference on machine learning*, pages 2649–2658. PMLR, 2018.
- F. Knechtli, M. Günther, and M. Peardon. *Lattice Quantum Chromodynamics: Practical Essentials*. SpringerBriefs in Physics. Springer Netherlands, 2016. ISBN 9789402409994. URL <https://books.google.co.uk/books?id=JgZODQAAQBAJ>.
- Alex Krizhevsky. Learning multiple layers of features from tiny images. Technical Report TR-2009, University of Toronto, 2009. URL <https://www.cs.toronto.edu/~kriz/learning-features-2009-TR.pdf>.
- Alex Krizhevsky, Ilya Sutskever, and Geoffrey E Hinton. Imagenet classification with deep convolutional neural networks. *Advances in Neural Information Processing Systems*, 2012.

- Zhouhan Lin, Roland Memisevic, and Kishore Konda. How far can we go without convolution: Improving fully-connected networks. *arXiv preprint arXiv:1511.02580*, 2015.
- Samuel Marks, Can Rager, Eric J Michaud, Yonatan Belinkov, David Bau, and Aaron Mueller. Sparse feature circuits: Discovering and editing interpretable causal graphs in language models. *arXiv preprint arXiv:2403.19647*, 2024.
- Callum McDougall. SAE Visualizer. [https://github.com/callummcdougall/sae\\_vis](https://github.com/callummcdougall/sae_vis), 2024.
- Kevin Meng, David Bau, Alex Andonian, and Yonatan Belinkov. Locating and editing factual associations in gpt, 2023.
- Beren Millidge and Sid Black. The singular value decompositions of transformer weight matrices are highly interpretable, Nov 2022. URL <https://www.alignmentforum.org/posts/mkbGjzxD8d8XqKHZA/the-singular-value-decompositions-of-transformer-weight>.
- Neel Nanda, Lawrence Chan, Tom Lieberum, Jess Smith, and Jacob Steinhardt. Progress measures for grokking via mechanistic interpretability, 2023a.
- Neel Nanda, Andrew Lee, and Martin Wattenberg. Emergent linear representations in world models of self-supervised sequence models, 2023b.
- Anh Nguyen, Jason Yosinski, and Jeff Clune. Multifaceted Feature Visualization: Uncovering the Different Types of Features Learned By Each Neuron in Deep Neural Networks, May 2016. URL <http://arxiv.org/abs/1602.03616>. arXiv:1602.03616 [cs].
- Chris Olah, Alexander Mordvintsev, and Ludwig Schubert. Feature visualization. *Distill*, 2017. doi: 10.23915/distill.00007.
- Chris Olah, Nick Cammarata, Ludwig Schubert, Gabriel Goh, Michael Petrov, and Shan Carter. Zoom in: An introduction to circuits. *Distill*, 5(3):e00024–001, 2020.
- William Peebles, John Peebles, Jun-Yan Zhu, Alexei Efros, and Antonio Torralba. The hessian penalty: A weak prior for unsupervised disentanglement. In *Computer Vision–ECCV 2020: 16th European Conference, Glasgow, UK, August 23–28, 2020, Proceedings, Part VI 16*, pages 581–597. Springer, 2020.
- Alec Radford, Jeffrey Wu, Rewon Child, David Luan, Dario Amodei, Ilya Sutskever, et al. Language models are unsupervised multitask learners. *OpenAI blog*, 1(8):9, 2019.
- Jürgen Schmidhuber. Learning factorial codes by predictability minimization. *Neural computation*, 4(6):863–879, 1992.
- Johannes Schneider and Michalis Vlachos. Explaining neural networks by decoding layer activations. In *Advances in Intelligent Data Analysis XIX: 19th International Symposium on Intelligent Data Analysis, IDA 2021, Porto, Portugal, April 26–28, 2021, Proceedings 19*, pages 63–75. Springer, 2021.
- Lee Sharkey, Dan Braun, and Beren Millidge. Taking features out of superposition with sparse autoencoders, Dec 2022. URL <https://www.alignmentforum.org/posts/z6QQJbtpkEAX3Aojj/interim-research-report-taking-features-out-of-superposition>.
- Mukund Sundararajan, Ankur Taly, and Qiqi Yan. Axiomatic attribution for deep networks, 2017.
- V. A. Traag, L. Waltman, and N. J. van Eck. From louvain to leiden: guaranteeing well-connected communities. *Scientific Reports*, 9(1), March 2019. ISSN 2045-2322. doi: 10.1038/s41598-019-41695-z. URL <http://dx.doi.org/10.1038/s41598-019-41695-z>.
- Dmitry Vaintrob, Jake Mendel, and Kaarel Hänni. Toward a mathematical framework for computation in superposition, Jan 2024. URL <https://www.alignmentforum.org/posts/2roZtSr5TGmLjXmNt/toward-a-mathematical-framework-for-computation-in>.

Jesse Vig, Sebastian Gehrmann, Yonatan Belinkov, Sharon Qian, Daniel Nevo, Simas Sakenis, Jason Huang, Yaron Singer, and Stuart Shieber. Causal Mediation Analysis for Interpreting Neural NLP: The Case of Gender Bias. *arXiv e-prints*, art. arXiv:2004.12265, April 2020. doi: 10.48550/arXiv.2004.12265.

Kevin Wang, Alexandre Variengien, Arthur Conmy, Buck Shlegeris, and Jacob Steinhardt. Interpretability in the wild: a circuit for indirect object identification in gpt-2 small. *arXiv preprint arXiv:2211.00593*, 2022.

Adam Yedidia. Gpt-2's positional embedding matrix is a helix, Jul 2023. URL <https://www.lesswrong.com/posts/qvWP3aBDBaqXvPNhS/gpt-2-s-positional-embedding-matrix-is-a-helix>.

Ziqian Zhong, Ziming Liu, Max Tegmark, and Jacob Andreas. The Clock and the Pizza: Two Stories in Mechanistic Explanation of Neural Networks. *arXiv e-prints*, art. arXiv:2306.17844, June 2023. doi: 10.48550/arXiv.2306.17844.

## A Models and datasets

Here we describe the models and datasets we use in the modular addition, CIFAR-10, and language model experiments. We also describe our slightly modified sequential transformer architecture.

### A.1 Modular addition

Our modular addition model follows [Nanda et al. \[2023a\]](#). It is a 1-layer decoder-only transformer with a residual stream width of 128, 4 attention heads of width 32, an MLP block of width 512 with ReLU activation, and no layer norm.

The dataset consists of sequences  $[x, y, =]$  where  $x$  and  $y$  are numbers from 0 to 112, and  $=$  is a constant. The labels (tested at the third position) are  $z = (x + y) \bmod 113$ ; we don't evaluate or compute the output at the first and second positions, as they do not affect the loss. The total dataset has  $113 \times 113 = 12769$  sequences; we use the first 30% to train the model and PCA/LIB, and the rest for testing.

We train the models with learning rate 0.001 (linear schedule with warmup), batch size 10,000, and the AdamW optimizer ( $\gamma = 1, \beta_1 = 0.9, \beta_2 = 0.98$ ). We train 5 models with different random seeds. The models are trained for 60,000 epochs, and we observe "grokking", i.e. a sharp decrease in test loss, after about a third of that time. All models achieve 100% accuracy on the train and test sets.

### A.2 CIFAR-10

Our CIFAR-10 [\[Krizhevsky, 2009\]](#) models are feedforward MLPs with two hidden layers. Each hidden layer has 60 neurons with a ReLU activation. We train 5 models that achieve 46.6% - 48.4% accuracy on the test set.

### A.3 Language models

For the language model tests we use pre-trained transformers. In this paper we show results for GPT2-small [\[Radford et al., 2019\]](#) and Tinstories-1M [\[Eldan and Li, 2023\]](#). Both models follow the GPT2 architecture, including layer norm. GPT2-small is the larger model with 85M parameters, 12 layers, and a residual stream width of 768. Tinstories-1M (1M parameters) has 8 layers and a residual stream width of 64.

We use the following datasets to run the LIB method: For GPT2 we use the openweb-text dataset [\[Gokaslan and Cohen, 2019\]](#), specifically a pre-tokenized version we host at `apollo-research/Skylion007-openwebtext-tokenizer-gpt2`. We run PCA on 50,000 sequences (51M tokens), and the second transformation of LIB (see Section 2.1) on Jacobians collected over 500 sequences (512,000 tokens), which takes on the order of 24 GPU-hours on A100 GPUs.

For Tinstories-1M we use the Tinstories dataset, again we host a pre-tokenized version (`apollo-research/skeskinen-TinyStories-hf-tokenizer-gpt2`). We use 99% of the dataset for the PCA, and 50,000 sequences (10M tokens) for the second transformation of LIB which is the limiting factor in terms of computational cost. We use the last 1% of the data as a test set.

### A.4 Sequential transformer

The LIB method assumes models to be sequential, i.e. each layer can be written as a function of the previous layer's output. To accommodate this, we make slight modifications to the transformer architecture that do not affect the computation, but simply the way we write the model. Essentially we make the residual stream an input to every layer that is just passed through to its output.

We show the resulting setup in Figure 15. The diagram shows a transformer block starting the the features before "ln in" (named `ln1`), the features between "ln in" and "ln out" (named `ln1_out`), and the features after "ln out" before the attention layer (named `attn_in`). The next three feature layers follow a similar pattern with `ln2`, `ln2_out`, and `mlp_in`. This is the naming convention we use in the feature visualizations hosted at [this url](#).

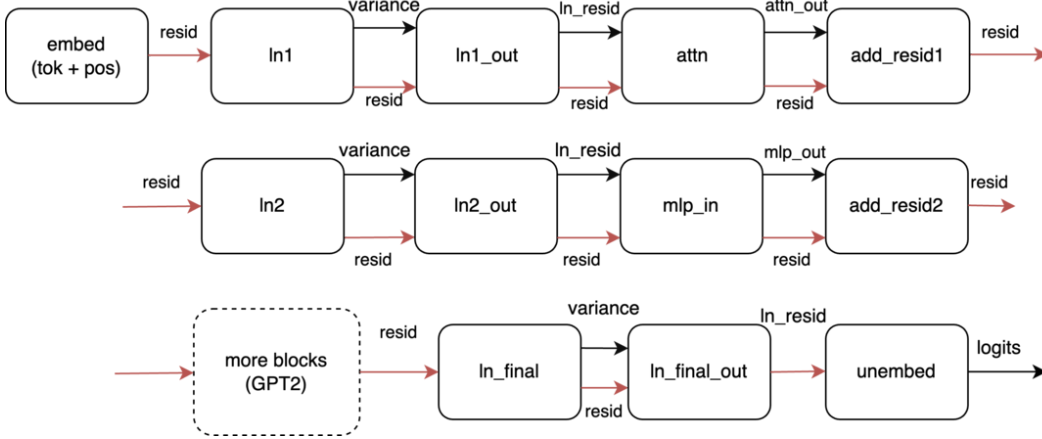


Figure 15: Sequential transformer.

### Layer norm treatment

Layer norm is a reasonably simple operation that (if handled naively) often appears messy and convoluted in LIB graphs. This is because every input feature affects the variance in the denominator of layer norm, and this denominator affects all output features. This all-to-all interaction can make it harder to disentangle modules.

In order to avoid this issue we split the layer norm module into two sections, where the “variance” used by layer norm is a hardcoded to be its own feature, and excluded from the LIB transformations.

The first part of layer norm (“In in”) just computes the variance and concatenates it to the residual stream. The second part of layer norm (“In out”) normalizes all other features by dividing by this variance. Splitting layer norm into two steps creates two simple layers rather than one complex layer, making the interaction graph more interpretable.

### A.5 Folding-in biases

It is mathematically convenient to consider a network without bias terms: this makes attribution easier as zero input results in zero output, and simplifies the mean centering by making it a linear operation.

In MLP and Transformer models, biases appear in the form  $\mathbf{f}^{l+1} = \text{act}(W^l \mathbf{f}^l + \mathbf{b}^l)$ , with the weight matrix  $W^l$ , the bias vector  $\mathbf{b}^l$ , and the activation function  $\text{act}$ . Throughout this paper we redefine the activations and weights as

$$\mathbf{f}^l = \begin{pmatrix} 1 \\ \mathbf{f}_{\text{orig}}^l \end{pmatrix} \in \mathbb{R}^{d^l+1} \quad \text{and} \quad W^l = \begin{pmatrix} 1 & 0 \\ \mathbf{b}_{\text{orig}}^l & W_{\text{orig}}^l \end{pmatrix} \in \mathbb{R}^{(d^{l+1}+1) \times (d^l+1)} \quad (5)$$

so that we can write the network without any biases as  $\mathbf{f}^{l+1} = \text{act}(W^l \mathbf{f}^l)$ .

## B Mathematical description of LIB transformations

We describe the LIB transformation as a PCA of the activations, and an SVD of the Jacobians. In this sections we provide a more detailed explanation of the LIB transformation, and equations to reflect our implementation accurately. We also provide pseudocode for the LIB and IG code in Appendix D.

We express the LIB linear transformation as a matrix,  $\hat{\mathbf{f}}^l = C^l \mathbf{f}^l$ , where  $\mathbf{f}^l$  is the vector of activations in layer  $l$  and  $\hat{\mathbf{f}}^l$  is the vector of activations in the LIB basis. We can factor this transformation into the two steps,  $C^l = C_{\text{SVD}}^l C_{\text{PCA}}^l$ . In the rest of this section we will derive how these transformations are composed until we arrive at the final equation for  $C^l$

$$C_{\text{PCA}}^l = (D^{l\frac{1}{2}})^+ U^l H^l, \quad C_{\text{SVD}}^l = \Lambda^{l\frac{1}{2}} V^l \quad (6)$$

$$C^l = \Lambda^{l\frac{1}{2}} V^l (D^{l\frac{1}{2}})^+ U^l H^l. \quad (7)$$

We will explain the individual components in the following sections.

### B.1 The first transformation

The first transformation implements a PCA of the activations in layer  $l$ . This consists of three steps: centering the activations, transforming them into a basis aligned with the principle components of the activations over the data set, and rescaling the basis directions to have a variance of 1.

Starting with the first step, we define the matrix  $H^l$  that centers the activations over the (training) dataset as

$$H_{jj'}^l = \delta_{jj'} - \mathbb{E}(f_j^l) \delta_{0j'} \quad (8)$$

We can write this as a single matrix because the activations include a constant column due to our bias-folding (appendix A.5).

Next we derive the principal components by solving the eigenvalue problem for the Gram matrix  $G^l$  of the centered activations. We obtain the diagonal eigenvalue matrix  $D^l$  and the orthogonal projection matrix  $U^l$ :

$$G_{jj'}^l := \frac{1}{|\mathcal{D}|} \sum_{x \in \mathcal{D}} (H^l \mathbf{f}^l(x))_j (H^l \mathbf{f}^l(x))_{j'} \quad (9)$$

$$G^l =: U^{lT} D^l U^l \quad (10)$$

Finally we use a multiplication by  $(D^{l\frac{1}{2}})^+$  to rescale the activations, and to remove near-zero PCA components. The  $+$  denotes the Moore-Penrose pseudo-inverse of  $D^{l\frac{1}{2}}$ . In the case of a diagonal matrix this gives another diagonal matrix with diagonal entries given by the reciprocal of the diagonal entries in the original matrix – unless the original entry was zero in which case the new entry is also zero. In our implementation of the pseudo-inverse, some principal components that are extremely close to zero ( $< 10^{-15}$  by default) are treated as exactly zero.

We obtain the intermediate result

$$\tilde{\mathbf{f}}^l = (D^{l\frac{1}{2}})^+ U^l H^l \mathbf{f}^l. \quad (11)$$

### B.2 The second transformation

The second transformation attempts to sparsify the interactions by aligning the basis of the activations in layer  $l$  with the basis in layer  $l + 1$ . We do this by performing an SVD of the Jacobians, the derivative of the activations in layer  $l$  with respect to the activations in layer  $l + 1$  for all data points.

To do this, we first compute the Jacobians

$$J_{ij}^l(x) := \frac{\partial f_i^{l+1}(\tilde{\mathbf{f}}^l(x))}{\partial \tilde{f}_j^l(x)} \quad (12)$$

obtaining a 3-tensor with dimensions  $(|\mathcal{D}|, d^{l+1}, d^l)$ . We flatten the first two indices and calculate the right-handed SVD (via eigendecomposing the gram matrix  $M$ ).

$$M_{jj'}^l := \frac{1}{|\mathcal{D}|} \sum_{x \in \mathcal{D}} \sum_{i=0}^{d^{l+1}} J_{ij}^l(x) J_{ij'}^l(x) \quad (13)$$

$$M^l =: V^{lT} \Lambda^l V^l. \quad (14)$$

In the eigendecomposition (14) we exclude the  $j = 0$  constant direction (responsible for mean centering) which we want to keep isolated and unchanged.

We obtain the orthogonal matrix  $V^l$  which transforms the activations into a basis aligned with the (right) singular vectors of the Jacobian, and the diagonal matrix  $\Lambda^{l\frac{1}{2}}$  which rescales the activations by how important they are for the next layer. We obtain the final activations as

$$\hat{\mathbf{f}}^l = V^l (\Lambda^{l\frac{1}{2}})^+ \tilde{\mathbf{f}}^l \quad (15)$$

$$= V^l (\Lambda^{l\frac{1}{2}})^+ (D^{l\frac{1}{2}})^+ U^l H^l \mathbf{f}^l. \quad (16)$$

### B.3 Recursive procedure

Since the second basis transformation depends on the basis chosen for the following layer, we calculate the LI basis recursively, starting from the final layer  $l_{\text{final}}$  and working backwards. At the final layer, we initiate the recursion with the PCA basis (without rescaling)

$$C^{l_{\text{final}}} := U^{l_{\text{final}}} H^{l_{\text{final}}}. \quad (17)$$

### B.4 Transformer implementation:

For transformers, the activations in a layer are a sequence of activations over the token dimension. In the first transformation we can simply treat the token dimension  $t$  just like the data dimension  $x$ , expanding the sum to

$$G_{jj'}^l := \frac{1}{T|\mathcal{D}|} \sum_{x \in \mathcal{D}} \sum_{t=1}^T (H^l f^l(x))_{j,t} (H^l f^l(x))_{j',t}. \quad (18)$$

For the second transformation we need to take into account that activations in adjacent layers at different token positions can depend on each other, so we need to compute the gradients for all combinations of token positions  $s, t$ . We again flatten the now 5-dimensional  $(x, s, i, t, j)$  Jacobian along all dimensions except for  $j$  to compute the right-handed (“ $j$ -sided”) SVD:

$$M_{jj'}^l := \frac{1}{T|\mathcal{D}|} \sum_{x \in \mathcal{D}} \sum_{s,t=1}^T \sum_{i=1}^{d^{l+1}} \frac{\partial \hat{f}_{i,s}^{l+1}(\tilde{\mathbf{f}}^l(x))}{\partial \tilde{f}_{j,t}^l(x)} \frac{\partial \hat{f}_{i,s}^{l+1}(\tilde{\mathbf{f}}^l(x))}{\partial \tilde{f}_{j',t}^l(x)}. \quad (19)$$

Transformers are typically represented as a residual stream with MLPs and attention components in parallel. For our method we want feature layers to represent a causal cut through the network, so we concatenate the activations of parallel components (in the standard basis) into a single vector  $\mathbf{f}^l$  before the LIB transformation. We illustrate this “sequential transformer” architecture in Appendix A.4.

## C Stochastic sources

Calculating the LIB basis, as well as the integrated gradient attributions, involves computing Jacobians between adjacent layers in the network (equations 2 and 19). This can be computationally expensive, especially for transformers, since their Jacobians have two hidden and two position indices and thus require calculating many entries.

### C.1 Stochastic sources in integrated gradient attribution

To make the calculation cheaper, we use stochastic source techniques (see e.g. chapter 3.6 in [Knechtli et al. \[2016\]](#) for an introduction). The idea is to not calculate the full Jacobian for each data point, but instead to calculate the gradient for a few random directions instead. We now demonstrate the derivation for the attribution calculation, the basis calculation is analogous. Equation (2) can be written as

$$\left( E_{i,j}^{l+1,l} \right)^2 = \frac{1}{|\mathcal{D}|} \frac{1}{T} \sum_{x \in \mathcal{D}} \sum_{s=1}^T A_{(i,s),j}^{l+1,l}(x) A_{(i,s),j}^{l+1,l}(x) \quad (20)$$

$$\text{with } A_{(i,s),j}^{l+1,l}(x) = \sum_{t=1}^T f_{j,t}^l(x) \int_0^1 d\alpha \left[ \frac{\partial}{\partial z_{j,t}^l} \left( F_{i,s}^{l+1,l}(\mathbf{z}^l) \right) \right]_{\mathbf{z}^l = \alpha \mathbf{f}^l(x)}. \quad (21)$$

We are computing all entries of the  $\mathbf{A}_{(i,s)}^{l+1,l}$  vector, but we do not care about the individual entries, only the sum of squares. This is a situation where stochastic sources can be applied. Intuitively this means, instead of calculating every entry of  $\mathbf{A}_{(i,s)}^{l+1,l}$ , we calculate the projection of this vector into a couple of random directions and sum these up instead.

Mathematically we express this as inserting an identity into equation (20) and replacing it with  $\delta_{s,s'} \approx 1/R \sum_{r=1}^R \phi_{r,s} \phi_{r,s'}$  where the sources  $\phi_r$  are random directions<sup>8</sup>, independently drawn for every  $r$  and every sample  $x$  from a distribution with mean zero and variance one

$$\left(E_{i,j}^{l+1,l}\right)^2 = \frac{1}{|\mathcal{D}|} \frac{1}{T} \sum_{x \in \mathcal{D}} \sum_{s=1}^T \sum_{s'=1}^T \delta_{s,s'} A_{(i,s),j}^{l+1,l}(x) A_{(i,s'),j}^{l+1,l}(x) \quad (22)$$

$$\approx \frac{1}{R} \frac{1}{|\mathcal{D}|} \frac{1}{T} \sum_{x \in \mathcal{D}} \sum_{r=1}^R \left( \sum_{s=1}^T \phi_{r,s}(x) A_{(i,s),j}^{l+1,l}(x) \right) \left( \sum_{s'=1}^T \phi_{r,s'}(x) A_{(i,s'),j}^{l+1,l}(x) \right). \quad (23)$$

The terms in brackets require the same number of gradient calculations as the original  $A_{(i,s),j}^{l+1,l}$  term

$$\left( \sum_{s=1}^T \phi_{r,s}(x) A_{(i,s),j}^{l+1,l}(x) \right) = \sum_{t=1}^T f_{j,t}^l(x) \int_0^1 d\alpha \left[ \frac{\partial}{\partial z_{j,t}^l} \left( \sum_{s=1}^T \phi_{r,s}(x) F_{i,s}^{l+1,l}(\mathbf{z}^l) \right) \right]_{\mathbf{z}^l = \alpha \mathbf{f}^l(x)}. \quad (24)$$

Thus using equation (23) over (2) changes the computational cost from  $\mathcal{O}(T^2)$  to  $\mathcal{O}(RT)$ . This approximation is exact only in the limit  $R \rightarrow \infty$ , but typically is good enough for  $R < T$  and thus reduces the computational cost significantly.

## C.2 Stochastic sources in LI basis computation

We apply the same approximation to the calculation of  $M$  in equation (19), and obtain

$$M_{j,j'}^l \approx \frac{1}{R} \frac{1}{|\mathcal{D}|} \frac{1}{T} \sum_{x \in \mathcal{D}} \sum_{r=1}^R \sum_{t=1}^T \sum_{i=1}^{d^{l+1}} \frac{\partial \left( \sum_{s=1}^T \phi_{r,s}(x) \hat{f}_{i,s}^{l+1}(\tilde{\mathbf{f}}^l(x)) \right)}{\partial \tilde{f}_{j,t}^l(x)} \frac{\partial \left( \sum_{s'=1}^T \phi_{r,s'}(x) \hat{f}_{i,s'}^{l+1}(\tilde{\mathbf{f}}^l(x)) \right)}{\partial \tilde{f}_{j',t}^l(x)}. \quad (25)$$

In this case we could also apply the stochastic sources approach to the sum over index  $i$ , either separately with two sets of sources, or by using the same sources for both sums. Testing the accuracy of this option however we found that the error due to stochastic sources was large, even when using  $R_i = d^{l+1}$  sources for the  $i$  index. Thus we use the full sum over  $i$  and stochastic sources only for the sum over  $s$ .

## C.3 Number of stochastic sources

In practice we find that using  $R = 1$  stochastic source is often sufficient. For MLP layers this is actually exact (because gradients between different positions are zero), and for attention layers we find that the error from using  $R = 1$  is typically small compared to the error introduced by the finite dataset size. We use  $R = 1$  in all experiments in this paper.

Most importantly, given a computational budget,  $R$  trades off directly against the number of data points  $|\mathcal{D}|$ , it is always better to use more data points than more sources. This is because increasing  $R$  samples the same datapoint with a new source, while increasing  $|\mathcal{D}|$  samples a new datapoint *and* a new source.

We can also see this tradeoff in the stochastic sources error estimator [Dong and Liu, 1994]

$$\sigma_{(E_{i,j}^{l+1,l})}^2 = \frac{2}{R} \frac{1}{|\mathcal{D}|} \sum_{r=1}^R \sum_{x \in \mathcal{D}} \frac{1}{T^2} \left( \sum_{s,s'=1}^T \left( A_{(i,s),j}^l(x) \right)^2 \left( A_{(i,s'),j}^l(x) \right)^2 - \sum_{s=1}^T \left( A_{(i,s),j}^l(x) \right)^4 \right) \quad (26)$$

which scales equally with  $1/R$  and  $1/|\mathcal{D}|$ .

<sup>8</sup>Specifically we use  $\phi_{r,s} \in \{+1, -1\}$  with equal probability. This has been shown to be optimal if we use no additional information [Dong and Liu, 1994].

## D Pseudocode for LIB and IG in transformers

In this section, we show pseudocode for calculating the LIB basis (see Section 2.1) and averaged attributions (see Section 2.2) in transformers. The pseudocode shows the non-stochastic version of the code, i.e. without stochastic sources explained in appendix C. We provide the full source code, with all functionality, at <https://github.com/ApolloResearch/rib>.

In the rest of the paper, matrix vector products are defined left to right, as in  $\hat{f}^l = C^l f^l$ , keeping with common mathematical convention. In this section, they are defined right to left instead, as in  $\hat{f}^l = f^l C^l$ , keeping with the Pytorch convention used in the code base. As a result, the ordering of matrices is often flipped compared to the definitions in the main text. Similarly, we define  $\hat{E}$  to be the RMS of attributions in the main text, but in the code base (and the pseudocode) we define  $E$  to be the sum of squares (without the square root).

### D.1 Local Interaction Basis in transformers

Algorithm 1 shows pseudocode for finding the Local Interaction Basis in a transformer. In the actual code base, we include the option to use stochastic sources in this algorithm to lower computing costs, see Appendix C.

---

**Algorithm 1** Pseudocode for finding the LI basis in Transformers.

---

**Output:** Returns interaction transformation matrix  $C^l$  in layer  $l$  for  $l \in \{0, \dots, l_{\text{final}}\}$

**for** layer  $l \in \{0, \dots, l_{\text{final}}\}$  **do**

$G^{l^l} \leftarrow \mathbf{0}_{(d^{l+1}, d^{l+1})}^l$

$H^l \leftarrow \mathbf{1}_{(d^{l+1}, d^{l+1})}^l$

**for**  $x$  in dataset  $\mathcal{D}$ ,  $t \in \{1, \dots, T\}$ ,  $j \in \{0, \dots, d^l\}$  **do**

$H_{j,-1}^l \leftarrow \frac{1}{|\mathcal{D}|T} \sum_{x,t} f_{x,t,j}^l$

$G_{j,j'}^l \leftarrow \frac{1}{|\mathcal{D}|T} \text{einsum}(\text{"xtj, xtj' \to jj'"}, f^l, f^l)$

**end for**

**end for**

**for** layer  $l \in \{l_{\text{final}}, \dots, 0\}$  **do**

$G^l \leftarrow H^l G^{l^l} (H^l)^T$

$D^l, U^l \leftarrow \text{eigendecompose}(G^l[1 :, 1 :])$

$U^l \leftarrow \mathbf{1}_{(d^{l+1}, d^{l+1})}^l$

$U^l[1 :, 1 :] = U^l$

**if**  $l == l_{\text{final}}$  **then**

$C^l \leftarrow H^l U^l$

**else**

$D^l \leftarrow \text{remove\_tiny\_eigenvals\_and\_diagonalize}(D^l)$

$M_{j,j'}^l \leftarrow \mathbf{0}_{(d^{l+1}, d^{l+1})}^l$

**for**  $x$  in dataset  $\mathcal{D}$ ,  $s, t \in \{1, \dots, T\}$ ,  $i \in \{0, \dots, d^{l+1}\}$ ,  $j \in \{0, \dots, d^l\}$  **do**

$J_{x,i,s,j,t}^l \leftarrow \frac{\partial(\sum_{i'} C_{i,i'}^{l+1} f_{x,i',s}^{l+1})}{\partial(f_{x,j,t}^l)}$

**end for**

$M_{j,j'}^l \leftarrow \frac{1}{|\mathcal{D}|T} \text{einsum}(\text{"xisjt, xisj't \to jj'"}, J^l, J^l)$

$M^l \leftarrow D^{l\frac{1}{2}} U^{lT} H^{l-1} M^l H^{l-1T} U^l D^{l\frac{1}{2}}$

$\Lambda^l, V^l \leftarrow \text{eigendecompose}(M^l[1 :, 1 :])$

$\Lambda^l \leftarrow \text{remove\_tiny\_eigenvals\_and\_diagonalize}(\Lambda^l)$

$V^l \leftarrow \mathbf{1}_{d^{l+1}, d^{l+1}}^l$

$V^l[1 :, 1 :] = V^l$

$C^l \leftarrow H^l U^l (D^{l\frac{1}{2}}) + V^l (\Lambda^l)^{\frac{1}{2}}$

**end if**

**end for**

---

## D.2 Edges in transformers

Algorithm 1 shows pseudocode to calculate the edges quantifying interaction strength between features in the Local Interaction basis in a transformer. In the actual code base, we include the option to use stochastic sources in this algorithm to lower computing costs, see Appendix C.

---

**Algorithm 2** Pseudocode for computing integrated gradient attributions in transformers.

---

**Output:** Returns interaction edges  $\hat{E}^l$  in layers  $l \in \{0, \dots, l_{\text{final}}\}$

**for** layer  $l \in \{0, \dots, l_{\text{final}} - 1\}$  **do**

$E_{i,j}^{l+1,l} \leftarrow \mathbf{0}_{(d^{l+1}+1, d^l+1)}$

**for**  $x$  in dataset  $\mathcal{D}$ ,  $s \in \{1, \dots, T\}$ ,  $i \in \{0, \dots, d^{l+1}\}$ ,  $j \in \{0, \dots, d^l\}$  **do**

$A_{x,i,s,j}^{l+1,l} \leftarrow \mathbf{0}_{(|\mathcal{D}|, d^{l+1}+1, T, d^l+1)}$

**for**  $\alpha \in \{0, \dots, 1\}$  (step size  $p$ ) **do**

$p' = 0.5p$  if  $\alpha = 0$  or  $\alpha = 1$  else  $p' = p$

$\hat{f}^{l+1}(\alpha \hat{f}^l)_{x,i,s} \leftarrow \left( f^{l+1}(\alpha \hat{f}^l(C^l) + C^{l+1}) \right)_{x,i,s}$

**for**  $t \in \{1, \dots, T\}$  **do**

$A_{x,i,s,j}^{l+1,l} += \text{einsum}(\text{"xisjt, xjt} \rightarrow \text{xisj"}, p' \frac{\partial(\sum_b \hat{f}^{l+1}(\alpha \hat{f}^l)_{x,i,s})}{\partial \alpha \hat{f}_{x,j,t}^l}, \hat{f}^l(X)_{x,j,t})$

**end for**

**end for**

$\hat{E}_{i,j}^l += \frac{1}{|\mathcal{D}|T} \sum_{x,s} \left( A_{x,i,s,j}^{l+1,l} \right)^2$

**end for**

**end for**

---

## E Alternative: Global Interaction Basis

In addition to the Local Interaction Basis (LIB) described in Section 2.1, we also experimented with what we call the Global Interaction Basis (GIB). This is an earlier variant of LIB proposed in Bushnaq et al. [2024a]. To compute the GI basis we adjust second transformation to align the basis of activations in layer  $l$  with the basis in the final layer  $l_{\text{final}}$  instead of layer  $l + 1$ . In practice we found similar results for the LIB and GIB, and thus focus on the LIB in the main text.

The difference is only in equation (13) which, for GIB, is

$$M_{jj'}^l := \frac{1}{|\mathcal{D}|} \sum_{x \in \mathcal{D}} \sum_{i=0}^{d^l_{\text{final}}} \frac{\partial \hat{f}_i^{l_{\text{final}}}(\tilde{\mathbf{f}}^l(x))}{\partial \hat{f}_j^l(x)} \frac{\partial \hat{f}_i^{l_{\text{final}}}(\tilde{\mathbf{f}}^l(x))}{\partial \hat{f}_{j'}^l(x)}. \quad (27)$$

### E.1 GIB results

We evaluated GIB on the modular addition and Tinstories-1M transformers. We found that the results were similar to LIB, resulting in similar sparsity and interaction graphs.

As an example we show the interaction graph for the modular addition transformer (seed-0) in Figure 16 for GIB and LIB. While the nodes are not exactly identical, the features are very similar and no graph is clearly more interpretable.

Performing the edge-ablation test for both bases we find that the GIB requires 131 and 82 edges across the attention and MLP layers, respectively. This is essentially identical to the LIB results (133 and 82 edges, respectively).

## F Fourier decomposition of activations in modular addition

In this section we briefly explain the Fourier decomposition we use to interpret the activations in the modular addition transformer. This is not a novel idea and has been commonly employed in the literature though we slightly improve on the representation used in Nanda et al. [2023a].

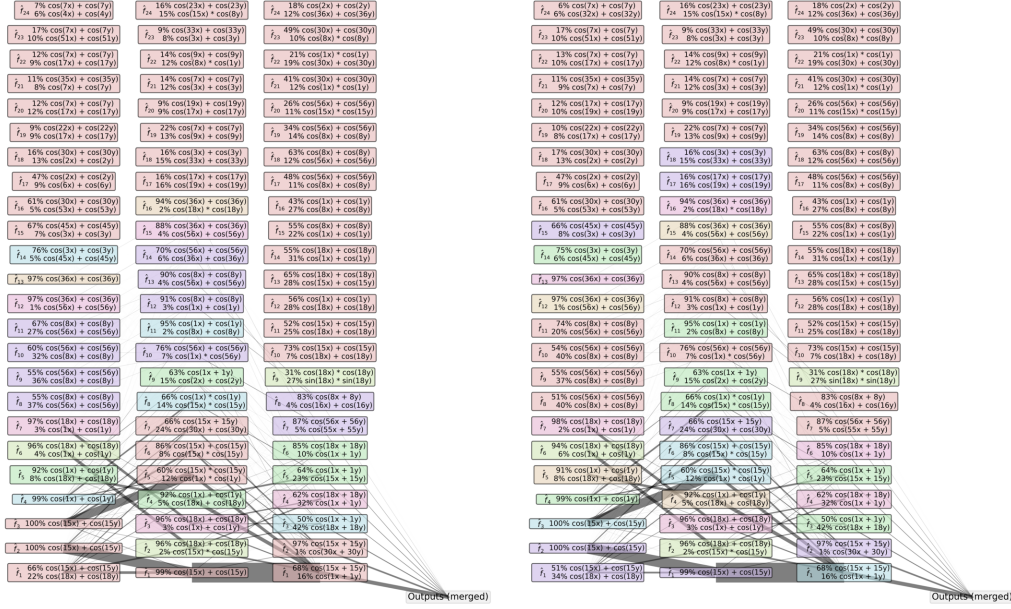


Figure 16: GIB (left) and LIB (right) interaction graph for the modular addition transformer (seed-0).

Fundamentally we can obtain the activations for all  $113^2$  possible inputs and plot the any activation as a function of  $x$  and  $y$ ,  $f(x, y)$ . However, the activations tend to be periodic in  $x$  and  $y$  due to the nature of this task, and it is more useful to apply a discrete Fourier transform (Fast Fourier Transform, FFT). The set of Fourier modes  $f'_{k_x, k_y}$  contains the same information as the original set of activations

$$f(x, y) = \sum_{k_x=-56}^{56} \sum_{k_y=-56}^{56} f'_{k_x, k_y} e^{2\pi i \frac{k_x x + k_y y}{113}}. \quad (28)$$

The Fourier modes  $f'_{k_x, k_y}$  tend to be sparse, i.e.  $f'$  is zero for most values of  $k_x$  and  $k_y$ . Thus we can describe (label) activations as a small list of frequencies. The rest of this section discusses how to transform the set of complex numbers  $f'_{k_x, k_y}$  into a list of sinusoidal terms.

First we separate the amplitude and phase information in  $f'_{k_x, k_y}$ . We write

$$f'_{k_x, k_y} e^{2\pi i \frac{k_x x + k_y y}{113}} = a_{k_x, k_y} e^{2\pi i \frac{\phi_{k_x, k_y}}{113} + 2\pi i \frac{k_x x + k_y y}{113}} \quad (29)$$

with real numbers  $a_{k_x, k_y}$  and  $\phi_{k_x, k_y}$ . Next we make use of the fact that that every non-zero frequency pair  $(k_x, k_y)$  has four sign variations in equation (28). Because the input activations  $f(x, y)$  were real, we know that  $f'_{k_x, k_y} = f'^*(-k_x, -k_y)$ , and thus  $a_{k_x, k_y} = a(-k_x, -k_y)$  and  $\phi_{k_x, k_y} = -\phi(-k_x, -k_y)$ . We can make use of these relations to turn equation (29) into a series of sinusoidal terms

$$\begin{aligned} f(x, y) &= a_{0,0} + \sum_{k_x=1}^{56} 2a_{k_x,0} \cos\left(2\pi \frac{k_x x + \phi_{k_x,0}}{113}\right) + \sum_{k_y=1}^{56} 2a_{0,k_y} \cos\left(2\pi \frac{k_y y + \phi_{0,k_y}}{113}\right) \\ &+ \sum_{k_x=1}^{56} \sum_{k_y=1}^{56} 2a_{k_x, k_y} \cos\left(2\pi \frac{k_x x + k_y y + \phi_{k_x, k_y}}{113}\right) + 2a_{k_x, -k_y} \cos\left(2\pi \frac{k_x x - k_y y + \phi_{k_x, -k_y}}{113}\right). \end{aligned} \quad (30)$$

Because all these terms are orthogonal we can compute the variance of  $f(x, y)$  that is explained by each term directly from their coefficients. As a shorthand notation we write  $\cos(k_x x + k_y y)$  to denote  $\cos\left(2\pi \frac{k_x x + k_y y}{113}\right)$ . We use this to label the features in the modular addition analysis, Section 3.1 and appendix G.

The  $k_x+k_y$  and  $k_x-k_y$  terms usually give a simple description of the activations, with one of the terms being zero. But sometimes we notice the respective coefficients have nearly the same value, with the same or with opposite signs. We notice that this corresponds to the trigonometric identities

$$\frac{1}{2}(\cos(x+y) + \cos(x-y)) = \cos(x)\cos(y) \quad (31)$$

$$\frac{1}{2}(\cos(x+y) - \cos(x-y)) = -\sin(x)\sin(y) \quad (32)$$

and thus dynamically switch from the  $\cos(k_x+k_y)$  and  $\cos(k_x-k_y)$  notation to the  $\cos(k_x)\cos(k_y)$  and  $\sin(k_x)\sin(k_y)$  notation when the latter provides a more sparse (more compressed) description.

## G More modular addition results

Here we show interaction graphs for all LIB and PCA runs on all 5 versions of the modular addition transformer. We show the RIB and PCA interaction graphs for seeds 0-4 in Figures 17 to 21. Each plot shows four layers (before attention, between attention and MLP, after MLP, and the output) and the nodes are sorted by the importance assigned by LIB or PCA, respectively. We label the nodes with feature index  $j$  as  $\hat{f}_j$  (for practical reasons we use  $\hat{f}$  labels for both LIB and PCA, but  $\hat{f}$  in the PCA plots corresponds to  $\tilde{f}$  in paper notation).

In these plots we show all features, including features which can be ablated while maintaining  $> 99.9\%$  accuracy (coloured in grey) that we exclude in the main text. We color the features by cluster, but do not change the sorting based on the clustering to allow for easier comparison. Additionally, we show the output layer and edges to it. Instead of showing all 113 output directions we combine them into a single node because the interactions to all output directions are roughly identical.

In these comparisons we want to highlight the observation mentioned in section 3.1.1, that some PCA features seem computationally-irrelevant—they do not connect to future layers. We expect this to happen whenever a direction is computationally-irrelevant but explains a significant amount of variance in the activations. LIB ignores such directions in activation space. We find this phenomenon in two categories of layers:

1. In feature layers just before a linear projection. For example the last layer before the unembedding (shown as the third column in the modular addition interaction graphs), or when we consider a layer right after the ReLUs (before the  $W_{\text{out}}$  projection). The failure here is in some sense trivial: yes, PCA doesn't know about the linear projection, but one could argue that one should run PCA after linear projections.
2. In layers that are *not* immediately before a linear projection. For example, the residual stream between the attention and MLP layers (second column in the interaction graphs). Our model here is that the residual stream has some leftover information that is not used in the following layers. This is a more interesting case as there is no simple fix for PCA.

We observe case 1 in all seeds of the modular addition transformer. Figures 17 to 21 all show features that are not connected to the outputs in the PCA basis.

Case 2 is less pronounced. We perform a manual inspection of the the first 25 features in the second layer (between attention and MLP) for all seeds and bases. We go through Figures 17 to 21 and count the number of features have incoming edges (as a proxy for assigned relevance) but no outgoing edges (as an indicator for functional relevance). This is a rough measure and we expect some false positives but we can compare the two bases. We indeed find more apparently-irrelevant features in the PCA basis (14) than in the LI basis (3). Concretely we find PCA features 17 to 20 in seed-0, 15 and 16 in seed-1, 17 and 24 in seed-2, 22 in seed-3, and 19 to 24 in seed-4 to be appear irrelevant. At the same time we find LIB features 18 in seed-0, feature 17 in seed-2, and feature 21 in seed-4 to be appear irrelevant.

## H More LLM feature vizualizations

Here we show three more LIB features, randomly selected from block 6 of the GPT2-small model.

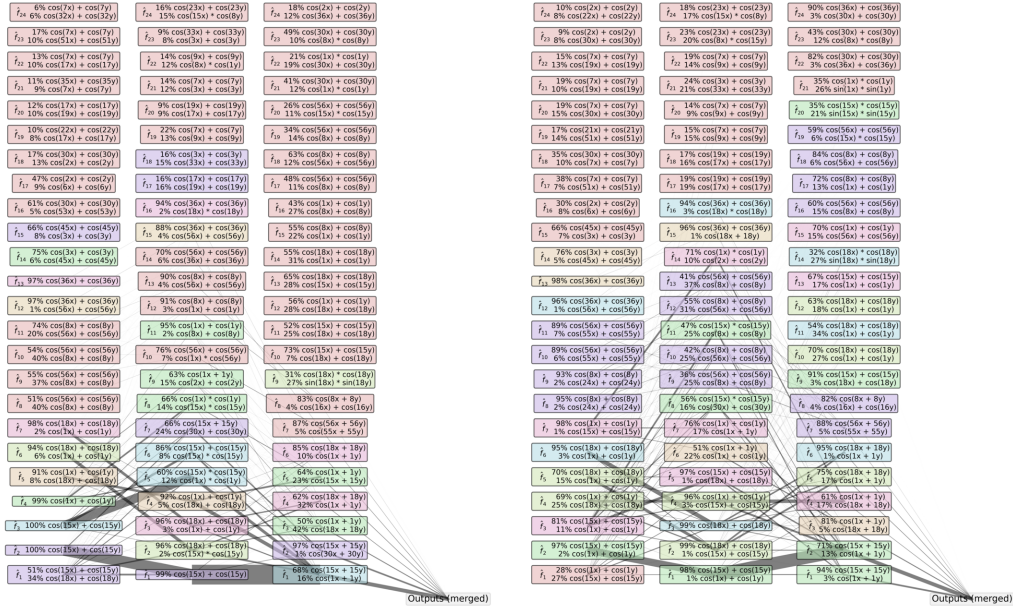


Figure 17: RIB (left) and PCA (right) interaction graphs of a modular addition transformer (seed-0).

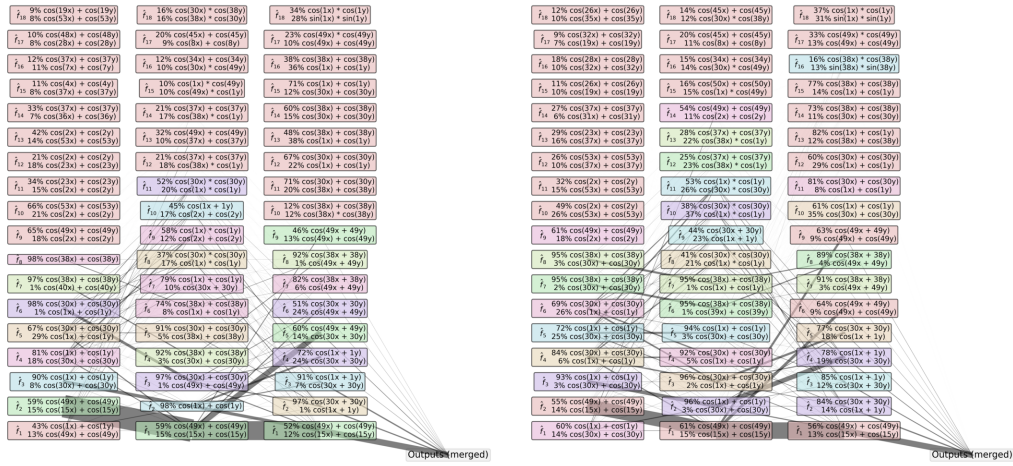


Figure 18: RIB (left) and PCA (right) interaction graphs of a modular addition transformer (seed-1).

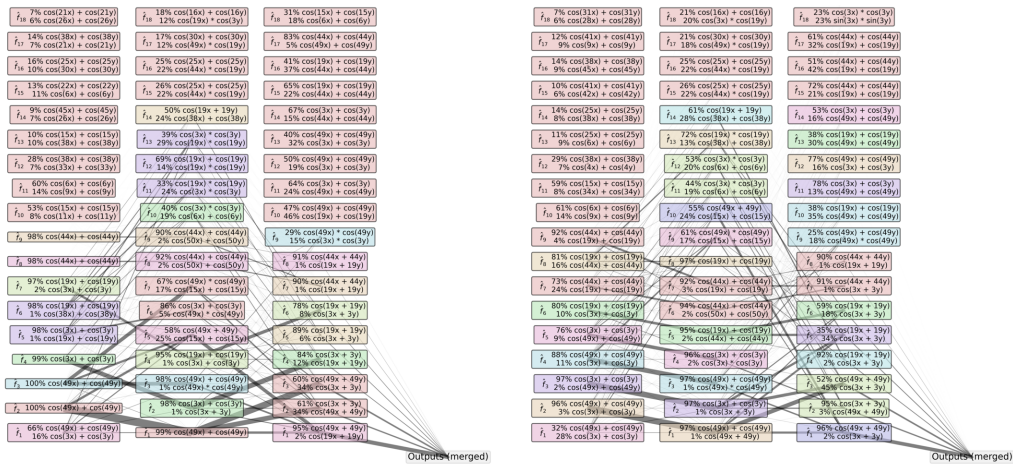


Figure 19: RIB (left) and PCA (right) interaction graphs of a modular addition transformer (seed-2).

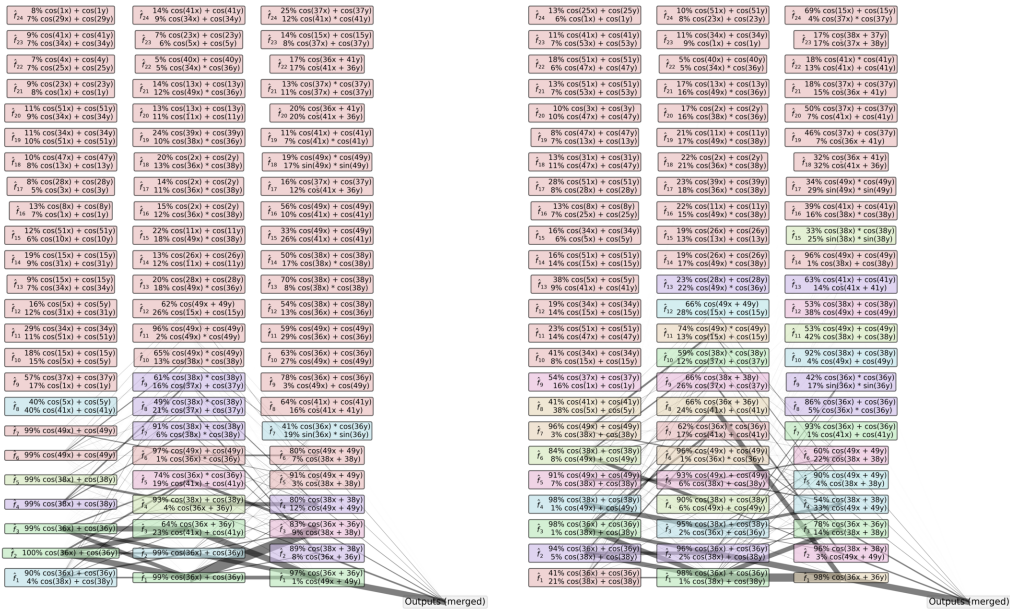


Figure 20: RIB (left) and PCA (right) interaction graphs of a modular addition transformer (seed-3).

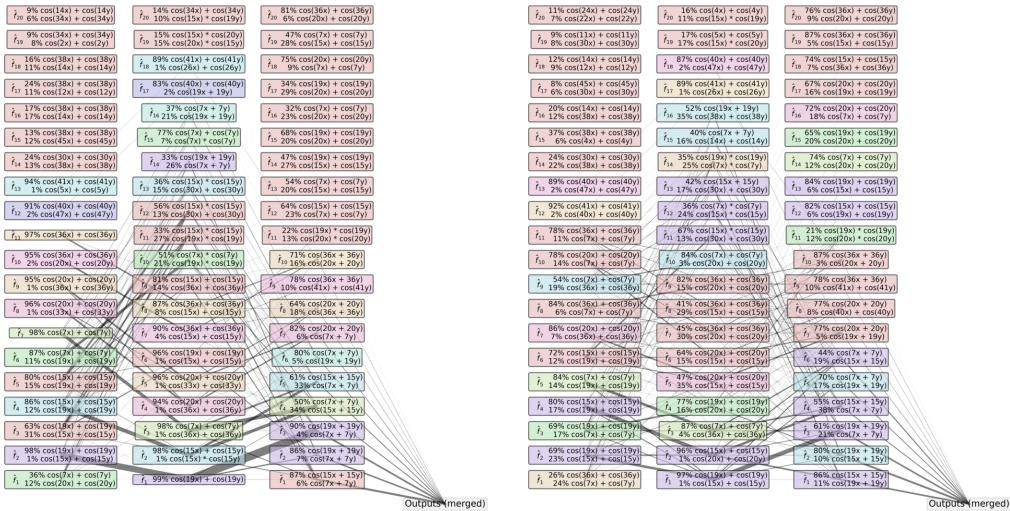


Figure 21: RIB (left) and PCA (right) interaction graphs of a modular addition transformer (seed-4).

1. Feature 82 does not appear to have a clear interpretation. Some dataset examples look similar, but there is no interpretation that explains a majority.

<p><b>TOP ACTIVATIONS</b> MAX = 3.760</p> <p>Pack), #88 - Ice Fields to teammates, opponents, coaches, owners, fan Maybe even compile a first aid box together. torching of homes, schools, offices, shops an the Myth. [51][54] The cat has been that can cause neurological and gastrointestinal son Ashish developed a breathing problem. Man shops, petrol pumps, schools, shopping malls, of possibility. 38. Red Dead Redemption. Prayers for them teachers tho. I</p>	<p><b>MIN ACTIVATIONS</b> MIN = -3.960</p> <p>It being fairly simple to 88, and partly due frosting. If you change the tip from a small functionality. sva info -p rt started tweeting about a Detroit Purse. Such On Tuesday, December 18, when Premier League Temple Address: 88hera, Gujarat 38. I know that every year I bring my 305 88d Puppy 88hera, 88 between threads. 88d Fried, our Board looks 1,165 voters from December 4th through 9th</p>	<p><b>INTERVAL 1.823 - 3.760</b> CONTAINS 0.754%</p> <p>Religious Identity Survey 1.5 million Estimate the problem facing the climate science and pol remove the source of the illness with little s . That was to be expected. But there are some usually is-was the entrance to the TTC station</p>	<p><b>INTERVAL -2.032 - -0.105</b> CONTAINS 43.235%</p> <p>favorite chess site: In-game replay correctly. Explain how to thread the bobbin: #64r research collaboration between labs in A of women and girls. Nominate an origin while avoiding its steep downside, you</p>
<p><b>TOP ACTIVATIONS</b> MAX = 2.312</p> <p>on to this president, 8 ceives from his fellow Demofrats cities like Benghazi and Misrata, where innoc his fellow Demofrats. At the are lightly fried and not deep fried! 6. Drai to see Annalise Abbie in a very vulnerable wa name is still a political in . It has a more bold than almond flour, which and a 31.8-metre distance from ing is the treatment Carter rec</p>	<p><b>MIN ACTIVATIONS</b> MIN = -2.075</p> <p>Now playing: watch this: Top 5 best . 88 Watch the moment unfold below: &lt;endofText&gt;Please enable Javascript to watch career Florida, left, watch election results including House Majority Whip Steve Scalise (f Under chain migration policies, immigrants gra .&lt;endofText&gt;Now playing: watch this: US Army of last year's Golden Globes, has been asked even set an alarm and watch as your Android p jagwar Records. Watch fan-shot footage of</p>	<p><b>INTERVAL -0.105 - 1.823</b> CONTAINS 55.548%</p> <p>Rico, to perform the test. 68 ys played with them in Adelaide. You'll were the bane of Wallace's short- allergic to. She doesn't cook. "I can skin lesions are hard to see. [117] Abr</p>	<p><b>INTERVAL -3.960 - -2.032</b> CONTAINS 0.463%</p> <p>'ve MacGyvered mental upgrades out of decades obbery, and have doubled down on their insiste radio as you go. Often you can pinpoint the m land on shelves beginning on August 22nd, but with an excellent slider after shifting to the</p>

2. Feature 304 seems to most strongly negatively activate on tokens related to watching, but this explanation does not generalize to intermediate or maximally positive activations.

<p><b>TOP ACTIVATIONS</b> MAX = 2.312</p> <p>on to this president, 8 ceives from his fellow Demofrats cities like Benghazi and Misrata, where innoc his fellow Demofrats. At the are lightly fried and not deep fried! 6. Drai to see Annalise Abbie in a very vulnerable wa name is still a political in . It has a more bold than almond flour, which and a 31.8-metre distance from ing is the treatment Carter rec</p>	<p><b>MIN ACTIVATIONS</b> MIN = -2.075</p> <p>Now playing: watch this: Top 5 best . 88 Watch the moment unfold below: &lt;endofText&gt;Please enable Javascript to watch career Florida, left, watch election results including House Majority Whip Steve Scalise (f Under chain migration policies, immigrants gra .&lt;endofText&gt;Now playing: watch this: US Army of last year's Golden Globes, has been asked even set an alarm and watch as your Android p jagwar Records. Watch fan-shot footage of</p>	<p><b>INTERVAL 1.215 - 2.312</b> CONTAINS 0.196%</p> <p>of fans who enjoy nothing more than slaughter: Kitchen owner, John Nguyen   Cajun Kitchen 88 living in an alternate reality. Those are t -&gt; 38/rain/82: 1 's truck leader, Today introduced the all-new</p>	<p><b>INTERVAL -0.978 - 0.318</b> CONTAINS 62.095%</p> <p>extend human consciousness throughout the univ who can we find to replace them", rather than is an interview with one of the largest anarc football coverage, has shown a highly unchara their company. I see this when I join Bourdai</p>
<p><b>TOP ACTIVATIONS</b> MAX = 1.483</p> <p>368 #88rpe: 100 Birth (31) Saw a turret from redemption ( Kin summit Manafort's attorneys say he should ( Kin summit Manafort's attorneys say he should ( /3 minutes until golden brown. These are light land man, convicted of vehicular homicide for: (153 yards and a touchdown), and then sometim , but it is only now that the former is truly B.V. All rights reserved.&lt;endofText&gt;On the talking to you. Why would you EVER want the g glass. #8Thank God for Zibohven in Springfield. Join the resistance? What if and a 1:2 touchdown-to-interception the Court of Appeal unanimously ruled last wee thinking "God, how could a guy do that?" the Liberal party. How can I be so sure? something that actually worked out Administrat 66s Anthony Brennan on Twitter: Sierra Studios Release Date: May 11, 2000</p>	<p><b>MIN ACTIVATIONS</b> MIN = -1.601</p> <p>wrote Show nested quote: on HTML https://www.881fasttelegaph.co Justice 1.23 Next All&lt;endofText&gt;=Republican is not meant to make fun of or demean the . 1.23 Next All&lt;endofText&gt;=This article 58 purakushi wrote Happy It worked materials to Jeffords and watch gear corps 68 And just last year, Michelle Dug Franky, I. myself, never witnessed any sexism As you (should) know, Eve Radio . Curiously, most liberals' readiness - COME. And just so man Sunj were Experimental subjects Three female rhesus mon olon was not a man accustomed to fear. haven't been lucky enough to get your hands his understanding of matters: It has become ev decided to do Shadow Demon Instead (whereas a : www.daily881.co.uk . https://www.881fasttelegaph.co , and built a runway capable of handling a 140</p>	<p><b>INTERVAL 0.118 - 1.215</b> CONTAINS 36.905%</p> <p>product - due to a handful of multinationals 6 cast in bronze, balance perfectly on opposite I created from the pull http://app sign the players when over the cap, functional See more Virtual Console games for Wii U.&lt;jen</p>	<p><b>INTERVAL -2.075 - -0.978</b> CONTAINS 0.750%</p> <p>algorithm and Northrop Grumman, the manufactu the institutional church, said Lauren Sandler, think Putin will be talked out of his decades: t uParticle = 8 ; uParticle &lt; Rouhani has shown he is listening, referring t</p>

3. Feature 477 does not appear to have a clear interpretation.

<p><b>TOP ACTIVATIONS</b> MAX = 1.483</p> <p>368 #88rpe: 100 Birth (31) Saw a turret from redemption ( Kin summit Manafort's attorneys say he should ( Kin summit Manafort's attorneys say he should ( /3 minutes until golden brown. These are light land man, convicted of vehicular homicide for: (153 yards and a touchdown), and then sometim , but it is only now that the former is truly B.V. All rights reserved.&lt;endofText&gt;On the talking to you. Why would you EVER want the g glass. #8Thank God for Zibohven in Springfield. Join the resistance? What if and a 1:2 touchdown-to-interception the Court of Appeal unanimously ruled last wee thinking "God, how could a guy do that?" the Liberal party. How can I be so sure? something that actually worked out Administrat 66s Anthony Brennan on Twitter: Sierra Studios Release Date: May 11, 2000</p>	<p><b>MIN ACTIVATIONS</b> MIN = -1.601</p> <p>wrote Show nested quote: on HTML https://www.881fasttelegaph.co Justice 1.23 Next All&lt;endofText&gt;=Republican is not meant to make fun of or demean the . 1.23 Next All&lt;endofText&gt;=This article 58 purakushi wrote Happy It worked materials to Jeffords and watch gear corps 68 And just last year, Michelle Dug Franky, I. myself, never witnessed any sexism As you (should) know, Eve Radio . Curiously, most liberals' readiness - COME. And just so man Sunj were Experimental subjects Three female rhesus mon olon was not a man accustomed to fear. haven't been lucky enough to get your hands his understanding of matters: It has become ev decided to do Shadow Demon Instead (whereas a : www.daily881.co.uk . https://www.881fasttelegaph.co , and built a runway capable of handling a 140</p>	<p><b>INTERVAL 0.712 - 1.483</b> CONTAINS 0.742%</p> <p>point increase from the year before.) These nur the timing off between the receiver and Russel driving a vehicle without an interlock device. group and vintage Cinelli handlebars and stem The Owner painter has an interface nearly iden</p>	<p><b>INTERVAL -0.830 - -0.059</b> CONTAINS 40.583%</p> <p>Just saw this tweet: Carlson is streaming live announced a plan for tobacco and nicotine reg. 03:21:55 BLR 2 Yauhen to shreds, it's ... well, else. On his way to a so-called leave</p>
<p><b>TOP ACTIVATIONS</b> MAX = 1.483</p> <p>368 #88rpe: 100 Birth (31) Saw a turret from redemption ( Kin summit Manafort's attorneys say he should ( Kin summit Manafort's attorneys say he should ( /3 minutes until golden brown. These are light land man, convicted of vehicular homicide for: (153 yards and a touchdown), and then sometim , but it is only now that the former is truly B.V. All rights reserved.&lt;endofText&gt;On the talking to you. Why would you EVER want the g glass. #8Thank God for Zibohven in Springfield. Join the resistance? What if and a 1:2 touchdown-to-interception the Court of Appeal unanimously ruled last wee thinking "God, how could a guy do that?" the Liberal party. How can I be so sure? something that actually worked out Administrat 66s Anthony Brennan on Twitter: Sierra Studios Release Date: May 11, 2000</p>	<p><b>MIN ACTIVATIONS</b> MIN = -1.601</p> <p>wrote Show nested quote: on HTML https://www.881fasttelegaph.co Justice 1.23 Next All&lt;endofText&gt;=Republican is not meant to make fun of or demean the . 1.23 Next All&lt;endofText&gt;=This article 58 purakushi wrote Happy It worked materials to Jeffords and watch gear corps 68 And just last year, Michelle Dug Franky, I. myself, never witnessed any sexism As you (should) know, Eve Radio . Curiously, most liberals' readiness - COME. And just so man Sunj were Experimental subjects Three female rhesus mon olon was not a man accustomed to fear. haven't been lucky enough to get your hands his understanding of matters: It has become ev decided to do Shadow Demon Instead (whereas a : www.daily881.co.uk . https://www.881fasttelegaph.co , and built a runway capable of handling a 140</p>	<p><b>INTERVAL -0.059 - 0.712</b> CONTAINS 58.336%</p> <p>phrase 88skin in the game 88 keeps popping 88instead of saying, black or black b back, that's really what Coinbase has done. A olan 41), Daly (Elworthy 54), Scott ( 'asting. Just as overweight and out of shape</p>	<p><b>INTERVAL -1.601 - -0.830</b> CONTAINS 0.338%</p> <p>66 Police have been making dozens of arrests i girls at Risk of genital Mutilation 647 devastating that even contemporaries, not unus ice sheet contains enough water to raise glob showing - followed by strong play in Cologne -</p>

## I More LLM Ablation Results

Here we present edge ablation results for all layers in the GPT2-small and Tinstories-1M models. Figure 22 shows the percentage of edges required (not ablated) to maintain a loss increase below 0.1 for all layers in the models.

In the attention and MLP layers we find the LIB to often beat PCA for GPT2-small (as shown in the main text), and LIB is sparser than PCA in all layers for Tinstories-1M. In the layernorm layers we find mixed and very different results, but we value the layernorm layers less because we mostly care about attention and MLP layers.

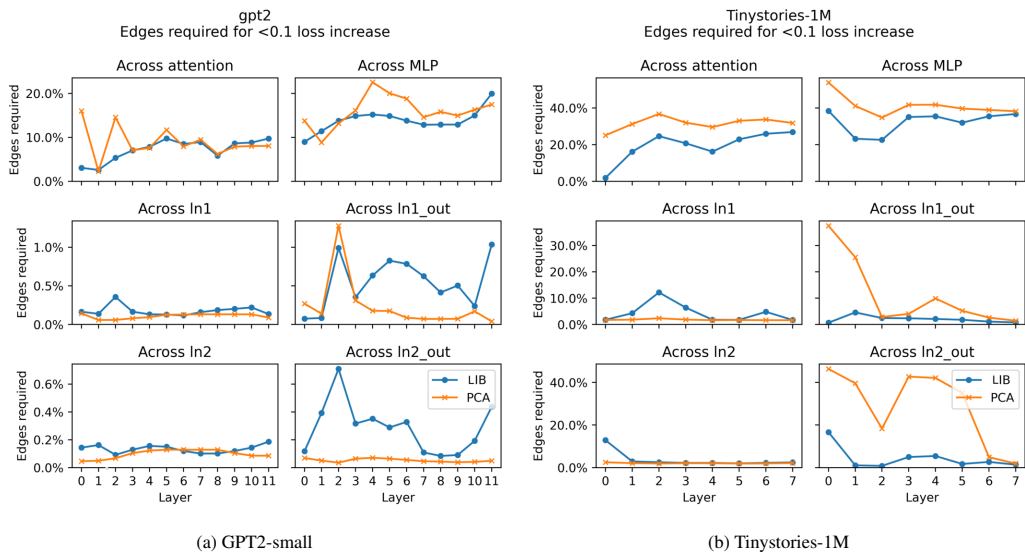


Figure 22: Edge ablation results on GPT2-small (left) and Tinystories-1M (right), for all layer types. Lower number of edges required is better, as it implies the graph is sparser.